Design of an Atmospheric Pressure Non-Thermal Miniature Plasma Jet and Exploration of its Potential as a Treatment for Cutaneous Leishmaniasis

Isabelle Christine Lacaille

Department of Chemical Engineering

McGill University

December 2013

A Thesis submitted to McGill University in partial fulfillment of the requirements of the degree of Master of Engineering

Acknowledgements

I would first like to express my deepest gratitude to both my supervisors, Dr. Sylvain Coulombe and Dr. Martin Olivier. Dr. Coulombe, thank you for believing in my potential those 3 years ago, and for giving me the chance to explore the world of academia. You taught me so much about research, engineering, teaching and keeping an eye on the big picture. Dr. Olivier, thank you for guiding me through the often dizzying world of immunology and microbiology, and for your inexhaustible enthusiasm. Without you, this multidisciplinary endeavor would not have been possible

I must also extend my gratitude to the trailblazers of this project, Dr. Valérie Leveillé, Ms. Sara Yonson and Dr. Mathieu Leduc, without whom this thesis could not have existed. My appreciation is also extended to Gerald Lepkyj and Frank Caporuscio for helping me with the initial stages of the project. I would also like to thank the members of the Plasma Processing Laboratory for your various helpful comments throughout the years, with a special thanks to Leron, my former summer research supervisor and former officemate. See you at graduation!

I must now express my very sincere gratitude to Marina Tiemi Shio and Caroline Martel for their extensive help with this project. Thank you for taking the time to show me all these laboratory techniques and for making me feel like a real member of the lab. Caro, I want to thank you for your help with the qRT-PCR, and for being an awesome lab mom. I also want to thank everyone from the 6th floor for everything you taught me, and for making me an honorary member of the exclusive immunology club.

None of this would have been possible without the support of my family. I must forever be grateful to my father, my mother, and my sister for supporting me throughout this project, my education, and all the rest. Thank you as well to the rest of my family and friends for your continued support. Thank you Kyriakos for your awesome engineering ideas and for your infallible moral support. I'm actually almost done now, I promise!

Finally, I must thank the following funding agencies and institutions: the Natural Sciences and Engineering Research Council of Canada (NSERC), the Canadian Institute for Health Research (CIHR), les Fonds de Recherche du Québec – Nature et Technologie

(FRQ-NT), les Fonds de la Recherche du Québec – Santé (FRQ-S), the Centre for Host-Parasite Interactions (CHPI), the Research Institute of the McGill University Health Centre (RI-MUHC), the Department of Chemical Engineering of McGill University through the Eugenie Ulmer Lamothe scholarship program.

Abstract

In recent years, there has been growing interest in developing non-thermal atmospheric pressure plasma (NAPP) devices for biomedical applications. Many of these applications are dependent on the production of nitric oxide (NO) and reactive oxygen species (ROS) by NAPP devices. These reactive species are bioactive molecules which have important and diverse roles in many types of cells and tissues. A potential application of NAPP devices that has yet to be explored is the topical treatment of cutaneous leishmaniasis (CL). Leishmaniasis is a neglected yet widespread disease in tropical and subtropical countries caused by the parasites of genus *Leishmania*. Inside human skin, *Leishmania* species infiltrate macrophages, cells which normally kill parasites and other pathogens by producing cytotoxic quantities of NO and ROS. *Leishmania* parasites are able to survive inside these cells by subverting their normal cell functions, including preventing NO and ROS generation. Hence, NAPPs could be used to treat CL by providing NO and ROS to the site of infection. The goal of this thesis is to investigate this possibility.

To that end, the atmospheric pressure glow discharge jet (APGD-j) was developed and used in both *in vitro* and *in vivo* experiments. Reactive species generation by the APGD-j was characterized using optical emission spectroscopy, demonstrating production of NO and ROS. A preliminary characterization of plasma treated cell culture media confirmed that NO transfers into the extracellular environment in an *in vitro* setting. The bone-marrow derived murine macrophage cell line B10R was used to assess the effects of the plasma on macrophage cell signalling and function. Treatments of the cells directly with the plasma and indirectly with plasma-treated media were shown to induce phosphorylation of p38, and the direct treatment also induced phosphorylation of JNK. These two proteins are part of the mitogen activated protein kinase (MAPK) family of signalling proteins involved in the immune response of macrophages which are down regulated by *Leishmania* infections. The translocation of the transcription factor downstream of these MAPK, activator protein 1 (AP-1), into the nucleus of the macrophage also increases following APGD-j treatment. Gene expression related to the macrophage immune response assessed 8 hours after indirect treatment. Out of 89 genes tested, 23 genes were modulated by the plasma treatment. The most notable change in

gene expression was a 27-fold upregulation of interleukin-1β (IL-1β), suggesting that the treatment has a pro-inflammatory effect on macrophages. Treating the Lm-LUC strain of *L. major* with the APGD-j resulted in cell membrane disruption and loss of metabolic activity in part of the population, demonstrating the toxic effects of the plasma treatment. Finally, APGD-j treatments of non-curing CL wounds of BALB/c mice significantly reduced the level of ulceration without affecting the parasite load in the skin. Together, these results suggest that although there is still work to be done regarding the optimization of the APGD-j for CL treatments, future generations of the device could potentially be used to minimize scarring and reduce recovery time of CL wounds.

Résumé

Au cours des dernières années, le domaine des applications biomédicales des plasmas non-thermiques a connu une croissance exponentielle. Plusieurs de ces applications dépendent de la production du monoxyde d'azote (NO) et des espèces réactives à base d'oxygène (ROS) à l'intérieur des plasmas. Ces espèces réactives ont une activité biologique, et elles ont des rôles importants et diversifiés dans de nombreux types de cellules et tissues humains. Une application potentielle des plasmas non-thermiques qui à date n'a pas encore été exploré en profondeur est le traitement de la leishmaniose cutané. La leishmaniose est une maladie négligée bien que très rependue mondialement dans les régions tropicales et subtropicales. Elle est causée par un parasite appartenant au genre *Leishmania*. A l'intérieur de la peau humaine, les espèces de *Leishmania* infiltrent les macrophages, des cellules qui normalement tuent les parasites et d'autres agents infectieux en produisant des quantités cytotoxiques de NO et des ROS. Leur survie dans ce milieu est possible grâce à leur capacité d'inhiber le fonctionnement normal des macrophages, y compris d'empêcher la production du NO et des ROS. Par conséquent, l'application d'un plasma non-thermique au site de l'infection pourrait aider à traiter la leishmaniose cutanée. L'objectif de cette thèse est d'étudier cette possibilité.

À cette fin, une source à jet de plasma non-thermique miniature opérant à atmosphérique, l'APGD-j, a été fabriquée et utilisée pour effectuer des expériences *in vitro* et *in vivo*. La production du NO et des ROS par l'APGD-j a été confirmée avec le spectre d'émission de la décharge électrique. Une caractérisation préliminaire des milieux *in vitro* a aussi confirmé le transfert du NO à l'intérieur du milieu extracellulaire. Une lignée de macrophages dérivés de la moelle osseuse murine nommé B10R a été utilisée pour effectuer des études sur l'effet des traitements de plasma sur la signalisation et le fonctionnement cellulaire des macrophages. Le traitement direct ainsi que le traitement indirect des cellules avec une solution de milieu cellulaire traité par l'APGD-j induit la phosphorylation du p38, et le traitement direct induit aussi la phosphorylation du JNK. Ces deux molécules sont des protéines kinases activées pas les mitogènes (MAPK), des protéines de signalisation qui sont désactivés suivant une infection à la leishmaniose. De plus, le traitement indirect des B10R induit la translocation de la protéine activatrice 1

(AP-1), un facteur de transcription en aval des MAPKs, vers l'intérieur du noyau. Ceci confirme l'activation de la cascade de signalisation associé au MAPK. L'expression des gènes associés aux fonctions immunitaires du macrophage a été évaluée. Des 89 gènes testés, 23 gènes ont été modulé par l'APGD-j. Le changement le plus important a été l'expression de Interleukine-1β (IL-1β), dont l'expression a augmenté 27 fois. Ce dernier résultat suggère que le traitement APGD-j a un effet pro-inflammatoire sur les macrophages. Le traitement de la lignée de promastigote Lm-LUC provenant de l'espèce *L. major* a entraîné une rupture de la membrane cellulaire ainsi qu'une perte de l'activité métabolique pour une fraction de la population, ce qui démontre les effets toxiques du traitement. Enfin, des lésions cutanées sur les peaux des souris BALB/c causées par l'administration des parasites de la lignée Lm-LUC ont été traitées avec l'APGD-j. Malgré que le nombre de parasites à l'intérieur du tissue n'a pas été affecté, le niveau d'ulcération des lésions a été réduit de façon significative. Ensemble, ces résultats suggèrent que même s'il y a encore du travail à faire en ce qui concerne l'optimisation de l'APGD-j pour cette application, les générations futures de l'appareil pourraient être utilisées pour minimiser les cicatrices et réduire le temps de récupération des lésions.

Table of Contents

Acknowledgements i

Abstract iii

Résumé v

Table of Contents vii

List of Figures x

Introduction 1

Chapter 1 : Literature review 3

1.1 Overview of processing plasmas 3

1.2 NAPP generation 3

1.3 Design considerations 5

1.4 Effects of NAPP on biological surfaces 6

1.4.1 Effect of plasma generated UV radiation 6

1.4.2 Effect of plasma generated RS 8

1.4.3 Effect of charged particles 9

1.5 Notable NAPP plasma devices 9

1.5.1 The Plasma Needle 10

1.5.2 The Floating Electrode Dielectric Barrier Discharge (FE-DBD) 11

1.5.3 The Plasma Pencil 13

1.5.4 The Atmospheric Pressure Glow Discharge torch (APGD-t) 15

1.6 Biological NO and ROS 16

1.6.1 Endogenous production of NO 17

1.6.2 Endogenous production of ROS 18

1.6.3 Biological functions of NO and ROS in the immune system 19

1.7 Cutaneous Leishmaniasis 21

1.7.1 Overview 21
1.7.2 Life cycle of *Leishmania* species 22
1.7.3 Clinical manifestation of CL 24
1.7.4 Treatments 24
1.7.5 Subversion of host immune response 25
Chapter 2 : Project Objective 28
Chapter 3 : Materials and Methods 29
3.1 Device & means of characterization 29
3.1.1 APGD-j 29
3.1.2 Optical Emission Spectroscopy (OES) 31
3.1.3 Nitrite (NO_2^-) assay 31
3.2 *in vitro* investigation 31
3.2.1 Cell culture 31
3.2.2 Plasma treatment of macrophages 32
3.2.3 Western Blot 32
3.2.4 Electrophoretic Mobility Shift Assay (EMSA) 33
3.2.5 Quantitative Reverse Transcription Polymerase Chain Reaction (qRT-PCR) 34
3.2.6 Plasma treatment of *L. major* promastigotes 34
3.2.7 Parasite viability assays 34
3.2.8 *in vitro* Infection and luciferase assay 35
3.3 *in vivo* investigation 35
3.3.1 *in vivo* infection and treatment of mice 35
3.3.3 Lesion Measurements 36
3.3.4 Measurement of parasite load 36
Chapter 4 : Results 37

4.1 Device characterization 37
4.1.1 OES 37
4.1.2 Nitrite concentration 38
4.2 Effect of *in vitro* plasma treatments on B10R macrophages 38
4.2.1 Cell signalling 38
4.2.2 Transcription factor translocation 40
4.2.3 Regulation of gene expression 41
4.3 Effect of *in vitro* plasma treatments on L. major 44
4.4 Plasma treatment of CL 46
Chapter 5 : Discussion 48
Chapter 6 : Conclusions and Future Perspectives 53
References 54

List of Figures

Figure 1.1: Paschen curves for several gases.[13] 4
Figure 1.2: (a) A cross-field jet and (b) a linear-field jet[16]. 6
Figure 1.3: The Plasma Needle. On the left, the plasma is seen generated at the tip. On the right, the plasma is formed between the needle and skin tissue[34] 10
Figure 1.4: FE-DBD applied to a thumb, demonstrating its non-thermal properties[41]. 12
Figure 1.5: The relatively long jet of the Plasma Pencil treating a biological surface[44]14
Figure 1.6: The atmospheric pressure plasma torch applied to a human thumb[48] 15
Figure 1.7: The production of NO during the different stages of wound healing[61] 20
Figure 1.8: Life cycle of *Leishmania species* [65] 23
Figure 1.9: Signalling cascade mediated by kinases and phosphatases[73] 26
Figure 3.1: Total and cross-sectional views of the APGD-j, along with a close-up of the plasma forming region. Dimensions are in inches. 30
Figure 4.1: Emission spectrum of the APGD-j. A) The absolute intensity UV-VIS emission spectrum. B) The relative intensity UV emission spectrum. Source and wavelength of spectral lines are indicated. 37
Figure 4.2: Nitrite concentration in RPMI following APGD-j treatment. Experiment performed in triplicate. Error bars represent standard deviation. 24-well plate: R2=0.96, P value<0.0001. 12-well plate: R2=0.98, P value<0.0001. 38
Figure 4.3: Direct and indirect plasma treatments of macrophages induce modulation of MAPK signalling. (A) Direct treatment at various treatment times (B) Indirect treatment at various incubation times (C) Time course following 10 minute direct treatment (D) Time course following 10 minute indirect treatment 39
Figure 4.4: Transcription factor AP-1 inside the nucleus after indirect plasma treatment 40
Figure 4.5: Viability of L. major following APGD-j treatment. (A) Representative experiment out of three biological replicates showing PI incorporation in treated cell populations. (B) Percentage of conserved cell membrane integrity as compared to the untreated sample. (C) Percentage of conserved metabolic activity as compared to the untreated sample. (D) Luciferase expression by internalized parasites 6 hours and 24 hours after the initial infection. Each column graph represents N=3 biological replicates

with experiment done in duplicated. Plasma treatments and their respective He controls were compared using the unpaired t-test. *, **, *** represent p<0.05, 0.01, 0.001 respectively. 45
Figure 4.6: Plasma treatments decelerate CL lesion growth without affecting parasite load in BALB/c mice infected with *L. major* (A) Weekly progression of lesion size. N=8 biological replicates up to week 5, with n=5 and n=6 for the helium and plasma groups on week 6, respectively. (B) The lesion areas on week 5 and (C) the parasite load at the experimental endpoint. ns, *, **, *** represent p>0.05, p<0.05, p<0.01, p<0.001 respectively, ... 46
Figure 4.7: The evolution of the average-sized helium and plasma lesions. 47

Introduction

Communication between various fields of research is vital to scientific progress. This is especially true in plasma science, where most research is based on exploiting the chemical and physical characteristics of plasmas for a wide range of applications. A growing field of research has emerged from one of these interdisciplinary collaborations: plasma medicine. The development of non-thermal plasma devices that operate at atmospheric pressure opened the door to plasma-biological surface interactions. Since then, a number of possible applications have been proposed, including sterilization of resistant bacteria, treatment of fungal infections, sterilization in oral care, treatment of surgical and chronic wounds, and even cosmetic treatments[1].

Perhaps the most ambitious goal of plasma medicine, the Holy Grail so to speak, is the development of plasma devices which can produce and deliver novel drugs in a clinical setting. To date, the best candidate for this objective is the production of nitric oxide (NO) and reactive oxygen species (ROS) for therapeutic applications. Despite their simplicity, these radicals have an important role in many biological functions, including regulation of blood flow, neuronal activity, and immune responses[2]. In recent years, many researchers in plasma medicine have shifted their focus towards designing plasma devices which can deliver these reactive species for therapeutic applications. Their studies have shown that non-thermal atmospheric pressure plasmas (NAPP) containing nitrogen (N_2) and oxygen (O_2) can successfully produce NO and ROS[3]. They also showed, through *in vitro* and *in vivo* testing, that the produced reactive species are able to interact with biological surfaces [4, 5].

The clinical applications of NAPP investigated thus far include sterilization of chronic wounds[6] and the treatment of tumors[7, 8]. However, another potential application, which has not received widespread attention, is the treatment of cutaneous leishmaniasis (CL). This condition is a cutaneous infection caused by *Leishmania*, a family of protozoan parasites. These parasites infect macrophages, immune cells which normally produce NO and ROS as part of the immune response. The parasites are able to survive inside the macrophages by subverting their normal cell function, which includes preventing the production of NO and ROS[9]. Thus, investigating the effect of NAPP

treatments on cutaneous leishmania could lead to a promising new application of NAPP in plasma medicine.

The purpose of the work presented herein was to explore the potential of NAPP as a treatment for CL. To this end, three specific goals were established. The first was to design and characterize a miniature NAPP device capable of delivering NO and ROS. The second was to study the effects of this NAPP on macrophage cells and leishmania parasites *in vitro*. The third was to study the effectiveness of NAPP as a treatment for CL wounds.

Chapter 1 : Literature review

1.1 Overview of processing plasmas

Simply put, plasma is the fourth state of matter. It is a gas that is partly ionized. It contains charged particles (electrons and ions), neutral particles (molecules and atoms) and photons. This gives plasmas a number of unique properties, including luminescence, high enthalpy, high reactivity and electrical conductivity. These properties are exploited in many different industrial processes, with the plasmas generated being tailored to specific applications.

In the plasma processing industry, there are two categories of plasmas: thermal and non-thermal plasmas. These are distinguished by their characteristic electron and heavy particle (neutral and ion) temperatures. Thermal plasmas are typically used for applications which require a high enthalpy, such as welding, plasma spraying and waste disposal. Non-thermal plasmas are used because their low temperature yet highly reactive media are ideal for the treatment of temperature-sensitive material, such as biological surfaces. Although there are thermal plasmas designed for biomedical applications[10, 11], these usually exploit the thermal properties of the plasma and are not suited for close range drug delivery applications.

1.2 NAPP generation

Plasma sources designed for biological surface interactions must operate at atmospheric pressure. However, NAPPs are difficult to generate. In plasma processing, plasmas are sustained by converting electrical energy from the mains to kinetic energy of the gas molecules. The applied electric field accelerates background electrons of the gas, which initiates a series of elastic and inelastic collisions. An elastic collision consists of a momentum transfer between particles. This type of collision is what causes the heavy particles to increase in temperature. Inelastic collisions cause ionization, excitation and other reactions between colliding particles. This type of collision is responsible for photon emission and the chemical reactivity of the plasma. The particle density and the power dissipated into the plasma will determine whether it is thermal or non-thermal. The

higher the power and particle density, the higher the rate of elastic collisions, and the closer the heavy particle temperature is to the electron temperature.

The electrical energy is provided by a power supply, which can deliver either direct current (DC) or alternating current (AC). The voltage required for plasma ignition, or breakdown of the gas, is dependent on the pressure multiplied by the distance between the electrodes (*pd*), a relationship illustrated by the Paschen curve, as seen in Figure 1.1. Typically, a minimum breakdown voltage of ~200V occurs at a *pd* product of 1 Torr·cm. At atmospheric pressure (p = 760 Torr), an inter-electrode spacing below 1 mm is required to reach low breakdown voltages[12]. Such distances are not practical for most intended source designs and thus, high voltages are often necessary.

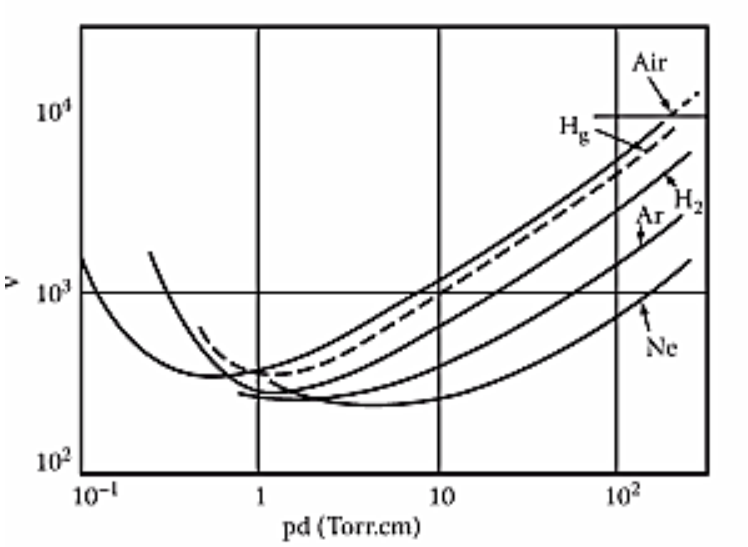

Figure 1.1: Paschen curves for several gases.[13]

In order to generate NAPP, techniques must be used to maximize the voltage while minimizing the power dissipated in the plasma. Examples of these include (1) limiting the transit time of the gas in the high electric field region by using a jet configuration, (2) cooling the fringes of the gas during generation (e.g. water cooling) (3) introducing a current-limiting component in the electrical circuit (4) pulsing the power and (5) miniaturizing the plasma device[12, 14]. Many of these techniques have been applied to the design of devices intended for biological surface interactions.

1.3 Design considerations

There are two principal device configurations for biological applications of NAPP. When the substrate acts as one of the electrodes, the configuration is said to be direct. When the plasma is formed between two electrodes and projected towards the substrate using a gas flow, it is said to be indirect[15]. The choice of either a direct or indirect configuration has important implications when it comes to interactions with biological surfaces. When a direct configuration is used, a current must pass through the substrate and a greater number of charged particles will be in contact with the substrate than with the indirect configuration. For the indirect configuration, if a gas flow is used to contact the plasma and the substrate, there will be the added effect of shear forces. Both configurations have previously been used to design plasma devices for biological surface interactions[15].

As stated in section 1.2, the inter-electrode spacing must be kept low in order to minimize the breakdown voltage. Despite this restriction, there are many options available for electrode design. For direct sources, the size and geometry of the live electrode will affect how much of the biological surface is treated. A small size is required for localized treatments, whereas a larger design facilitates covering larger surface areas. For indirect sources, the position of the electrodes will determine the direction of the electric field, thus affecting the location of the plasma. A popular design is the use of concentric cylindrical electrodes, with the plasma gas flowing between them. This induces an electric field which is perpendicular to the gas flow in the radial direction. This configuration is also known as a cross-field jet. Another is to have the two electrodes positioned such that the electric field is generated in parallel to the gas flow. This configuration is called the linear field jet. A comparison of these two configurations is shown in Figure 1.2, and their characteristics are reviewed by Walsh and Kong[16].

Four well documented examples covering all these design options are the Plasma Needle, the Floating Electrode DBD (FE-DBD) the Plasma Pencil and the Atmospheric Pressure Glow Discharge torch (APGD-t). These devices, along with their contribution to the field of plasma medicine, will be reviewed in section 1.5.

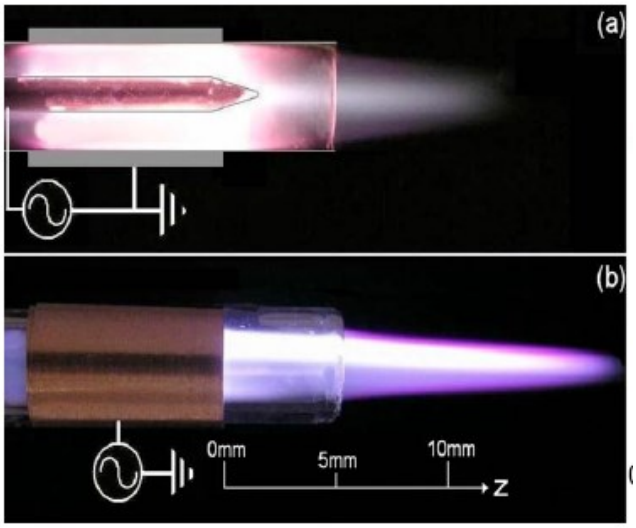

Figure 1.2: (a) A cross-field jet and (b) a linear-field jet[16].

1.4 Effects of NAPP on biological surfaces

Plasmas have been shown to have an effect on both prokaryotic and eukaryotic cells. Biological entities which have been treated with NAPPs include bacteria, spores, biofilms, plants and mammalian cells[15]. The main motivation for studying interactions between plasmas and prokaryotic cells is to investigate sterilization applications. These include the sterilization of abiotic surfaces such as hospital equipment, and of biological surfaces such as plants, foods and animal and human tissues. Plasma interactions with eukaryotic cells are studied once again for sterilization applications, but also for various other applications including modulation of cell adhesion, induction of apoptosis in cancer cells and enhancement of blood coagulation. One of the most challenging aspects of plasma medicine research is differentiating the effects of different plasma characteristics. These can include heat, shear stress, ultra-violet (UV) radiation, reactive species (RS) and charged particles. For NAPPs, the plasma parameters of interest are UV radiation, RS and charged particles [1, 15].

1.4.1 Effect of plasma generated UV radiation

UV radiation is generated in plasmas when high energy photons (λ<400 nm) are emitted by excited species experiencing an electron transition to a lower energy level. There are three categories of UV radiation, UVA (400-315 nm), UVB (315-290 nm) and UVC (280-100 nm), the latter having the strongest bactericidal effect on biological

surfaces[17]. There are two ways in which UV radiation can lead to cellular damage: directly through the absorption of UV radiation by macromolecules, and indirectly by inducing the release of intracellular RS. Examples of direct damage include DNA modification and the rearrangement and aggregation of polypeptide chains of proteins. Indirect UV damage through release of RS include oxidative degradation of lipids and DNA damage[1]. UV radiation damages prokaryotic cells more than eukaryotic cells, which have a nucleotide excision repair system. However, chronic exposure of eukaryotic cells to UV leads to DNA damage due to errors in the repair system[1]. Therefore, plasma devices designed for treatment of mammalian tissue should produce a limited the amount of UV radiation. However, in the context of wound healing, the bactericidal effects of a treatment are desirable, since they prevent further infection and accelerate the healing process[18].

There is some debate in literature concerning the importance of UV radiation during NAPP treatment of biological surfaces. In one study, the UV radiation generated by the plasma source was found to be responsible for short-term sterilization of bacterial suspensions. In media with high UV transparency (Phosphate Buffered Saline (PBS), which demonstrated a transparency above 70% UV), treating the suspension with plasma generated UVs through a quartz glass had the same effect as treating the suspension with the microwave plasma jet directly. However, it was shown through incubation of the suspensions that the long term bacterial growth inhibition was due to RS plasma products which had diffused into the media[19]. Several other studies argue that UV radiation does not play a significant role in inactivation of prokaryotes. Some of these point to the fact that their plasma device does not generate significant UV radiation in the lethal range [20-24]. Others physically separate the reactive and charged plasma species from the UV radiation using UV transparent material and show that the sterilization effects are significantly reduced[25, 26]. This discrepancy can be explained by the great variation in excitation modes and gas compositions of the plasma sources used for experimentation. Given particular experimental conditions, excited species can be generated in the plasma which emit very strongly in the germicidal UV range. Of particular interest to this project is a study by Boudam *et al*, which demonstrates that a high intensity peak in NO_γ band system emission (200-285 nm) can be achieved in a N_2-N_2O plasma at a very narrow

range of N_2O on the order of 40 ppm. They note that at atmospheric pressure, this peak is especially narrow and can easily be missed[27]. This has an important consequence for plasma devices intended for NO generation: NO rich plasmas will emit very strongly in the UVC range and thus have strong bactericidal effects.

1.4.2 Effect of plasma generated RS

Mammalian cells produce RS as part of their natural antibacterial and antiviral defence mechanisms, and also play a role in cellular function. They have been shown to have important roles in signalling pathways, mainly through altering the intracellular redox state, or by oxidation of signalling proteins. On a cellular level, this means RS regulate differentiation, division, migration and apoptosis, with the ultimate effect on cells being determined by the type and dose of RS[1]. Examples of RS present in plasma which have been shown to have these types of effects are NO, hydroxyl radical (OH), atomic oxygen (O), ozone (O_3), O_2 metastable states, hydrogen peroxide (H_2O_2) and superoxide (O_2^-). Not only does the dosage of these RS regulate the effect they have in unicellular and multi-cellular systems, but the interplay between the RS is also of high significance. Examples of synergy between RS include NO and superoxide, the latter scavenging NO to induce blood coagulation, and NO with H_2O, which depending on the concentration of the two can either inhibit or induce cell apoptosis[1].

There is a significant amount of evidence in literature supporting the case for RS as a major player in plasma interactions with both prokaryotic cells and eukaryotic cells. Many studies have shown that the sterilization of bacteria and spores with their plasma devices is primarily due to intracellular oxidative stress induced by reactive oxygen species[24, 26]. Reactive species have also been identified as the main cause of proliferation at low doses and DNA damage at higher doses leading in apoptosis of mammalian cells[28]. Only recently have studies begun examining the role of specific reactive species during plasma-cell interactions. One study used wild type *E. coli* and *E. coli* mutants lacking certain genes to evaluate the importance of specific plasma-induced stresses. It was found that UV-radiation and OH radicals had a minimal contribution to bacterial inactivation, with the important species being narrowed down to NO and superoxide producing agents[29]. In another study, results from emission spectroscopy

combined with oxidation and lipid peroxidation assays led to the conclusion that NO, which readily diffuses into cells, was responsible for intracellular oxidation of HeLa cells[30]. Another studied the mechanisms of plasma induced apoptosis in human hepatocytes (HepG2) cancer cells by monitoring the concentrations of intracellular and extracellular NO and reactive oxygen species (ROS). It was determined that the diffusion of NO into the cells caused an increase in intracellular ROS, in turn causing increased oxidative stress and lipid peroxidation, finally resulting in apoptosis[31].

1.4.3 Effect of charged particles

Of the three plasma parameters which have an effect on biological surfaces, charged particles are the easiest to control when studying plasma-cell interactions. This is due to the fact that the recombination of charged particles and electrons outside of the main plasma volume occurs fast enough to conclude that these do not reach the surface in indirect treatments. Therefore, charged particles only come into play when the direct configuration is used, that is, when the biological surface acts as one of the electrodes, and thus are placed in direct contact with the plasma. Although not as prominently studied as RS and UV radiation, charged particles have been proposed to contribute to cell interactions with direct plasma. It is suggested by Laroussi *et al* that the cell lysis of *E. coli* is caused by the negative charging and subsequent electrostatic disruption of the cell membrane[32]. A further contribution is made by Stoffels *et al*, who note that the electric double layer of the cell wall can cause it to become disrupted by charging, with death resulting for cytoplasm leakage rather than complete cell lysis[15]. They also note that eukaryotic cells are resistant to this type of disruption.

1.5 Notable NAPP plasma devices

As discussed in section 1.3, there are many possible design strategies for NAPP production, and the chosen design can strongly affect the characteristics of the plasma generated and subsequently, its interaction with biological surfaces. As seen in section 1.4, this can lead to many conflicting results regarding which plasma parameter dominates the interaction. Since every research group generally develops its own device, a thorough understanding of the design is required to critically analyse the results of the research done by the group. The following describes a small sample of the devices which

can be found in plasma medicine literature. These were chosen because (1) they are well characterized, (2) the interactions studied using these sources contributed significantly to the field and (3) together, they demonstrate the large variation in possible designs of NAPP for biological surface treatments.

1.5.1 The Plasma Needle

The Plasma Needle consists of a tungsten wire 3 mm in diameter, 5 cm in length, encased in a Perspex tube. The plasma is generated at the tip of the wire using an RF power supply, at a frequency of approximately 10 MHz. Helium (He) gas purges the casing of air in order to facilitate breakdown. Since breakdown is also facilitated by the sharp geometry of the needle, the plasma can be kept non-thermal, with power dissipated in the plasma around 100 to 180 mW. The root mean square of the sustaining voltage is of 140-270 V. A complete electrical and optical characterization of the device was performed by Kieft *et al*, in which the impedance of the device was measured, the electron density was estimated and reactive species generated due to air entrainment into the casing were identified[33].

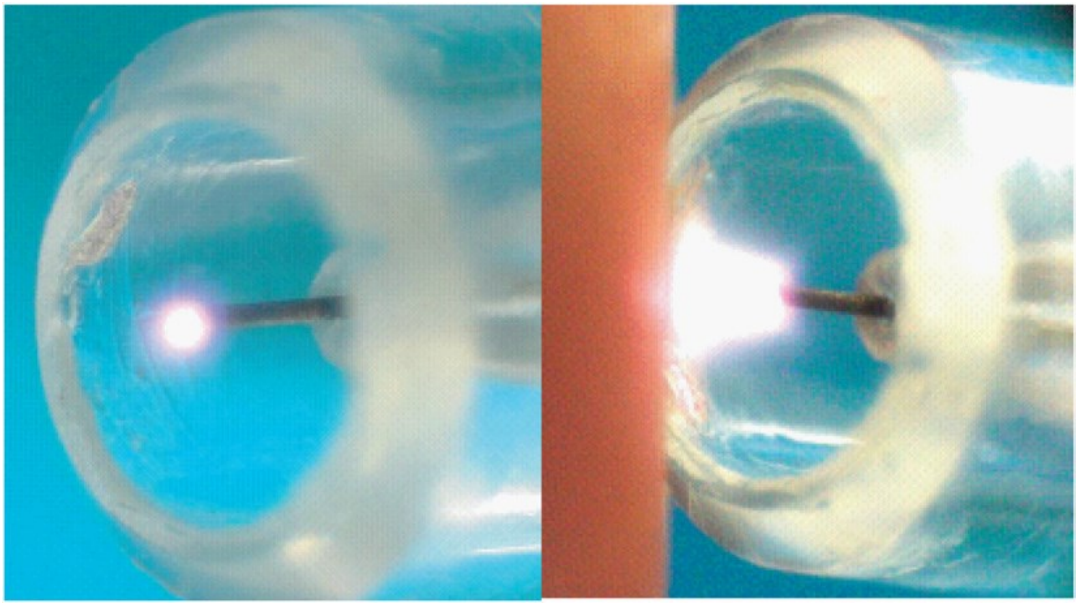

Figure 1.3: The Plasma Needle. On the left, the plasma is seen generated at the tip. On the right, the plasma is formed between the needle and skin tissue[34]

Since the Plasma Needle was the first atmospheric pressure plasma designed as a tool for biomedicine, there have been numerous studies performed with this device. Notable

among these are the studies on bacteria inactivation[35, 36], biofilm inactivation[37], mammalian cell detachment and apoptosis[34, 38, 39], and smooth muscle cell necrosis and endothelial cell apoptosis through a gas permeable membrane[40]. It was demonstrated that the plasma needle is capable of inactivating bacteria in a site specific manner, with 10^4-10^5 colony forming units being deactivated after a treatment time of 10 seconds at 180 mW. In the case of biofilms deactivation as an application in dental procedures, it was shown that a treatment time of one minute at 100 mW effectively inactivates a *Streptococcus mutans* biofilm, however in the presence of sucrose the biofilm regrows. Stoffels *et al* demonstrated that at a low power level (100 mW), mammalian cells do not experience necrosis, but rather detach and are able to reattach within a few hours, and thus transferred to a new plate. This was initially attributed to the interaction of RS with adhesion molecules between cells. However, it was later proposed that detachment was caused by an electrostatic interaction between the plasma and the cells, as the presence of a gas permeable membrane completely eliminated the detachment effect of the plasma.

1.5.2 The Floating Electrode Dielectric Barrier Discharge (FE-DBD)

Principle of operation of the FE-DBD is that of a DBD. These are among the first NAPP developed and studied in literature. A continuous or pulsed high voltage is applied to two electrodes insulated with a dielectric material. The dielectric material prevents current from building up, keeping the plasma non-thermal. Fridman *et al* adapted this design to incorporate the biological surface, living tissue or otherwise, as one of the electrodes. These biological surfaces have a high dielectric constant and therefore a high capacity for charge storage. Given the fact that the treated surface remains ungrounded, the group has termed this surface the “floating electrode”[41].

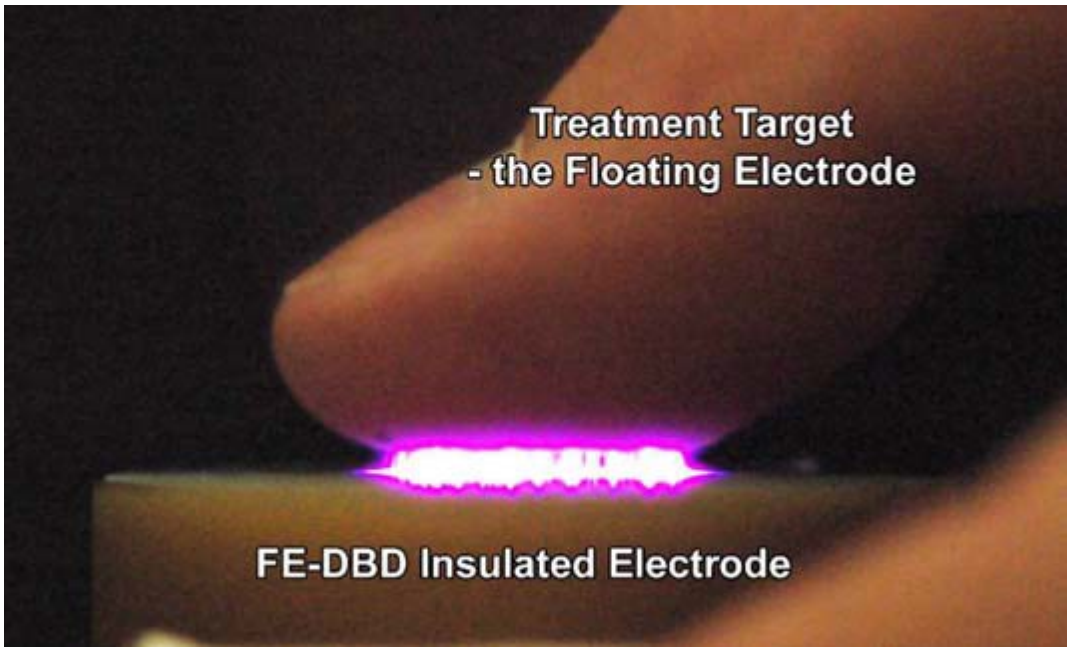

Figure 1.4: FE-DBD applied to a thumb, demonstrating its non-thermal properties[41]

Many electrode configurations were developed, with the most common being a round electrode of 25.4 mm in diameter. The dielectric used is polished fused quartz with a thickness of 1 mm. The discharge is ignited by applying a continuous high voltage (10-30 kV) wave to the live electrode, with the air between the electrode and the treatment area breaking down when the gap between them reaches approximately 3 mm. The power density applied to the surface is usually between 0.1 to 2 W/cm^2[42].

Among the studies performed with this device were on the effects of the FE-DBD on blood coagulation and tissue sterilization[4, 41], apoptosis of melanoma cell lines[42], endothelial cell proliferation[43], and DNA damage to mammalian breast epithelial cells[28]. Treatments of blood samples *in vitro* and *in vivo* with the FE-DBD have demonstrated that accelerated blood coagulation takes place. Although the exact mechanism of this acceleration is unknown, it was supposed that this was due to interaction of plasma species with fibrinogen, a protein involved in the final stages of coagulation. In the skin sterilization study, it was found that a treatment time of 6 seconds was required for hospital-grade sterilization, while no visual or microscopic damage of the tissue was observed for a treatment time of up to 5 minutes. A “maximum acceptable dose” was determined at 10 minutes of a 0.6 W/cm^2 treatment, and 40 seconds at 2.3

W/cm^2. The treatment of melanoma cell lines revealed that at a power density of 0.8±2 W/cm^2, the cells demonstrated necrosis as well as apoptotic behavior, with apoptosis alone being responsible for cell death at treatment times under 5 minutes. In the study of plasma treated endothelial cells, cells treated at low power fluxes (0.1W /cm^2) exhibited a 2 fold increase in proliferation, associated with an increase in fibroblast growth factor-2 (FGF2) production by the cells. Inhibiting FGF2 using neutralizing antibodies and ROS scavengers demonstrated that the proliferative effect of the plasma treatment was due to ROS-mediated increase of FGF2. Finally, DNA damage in mammalian breast epithelial cells resulting from plasma exposure was shown to have been mediated by exogenously introduced and endogenously produced intracellular ROS. Interestingly, it was shown that plasma treating the cell culture medium separately would affect the cells in the same way as treating the cells in the medium directly. This was true even when holding the treated medium for up to one hour before introducing the cells. After introducing specific amino acids and recorded peroxidation efficiency, researchers noted that there was a direct correlation with the amount of DNA damage. This led them to believe that the formation of stable organic peroxides in the treated medium resulted in the ability of the medium to conserve its DNA damaging ability long after plasma treatment.

1.5.3 The Plasma Pencil

The Plasma Pencil is designed to produce a long plasma jet and thus provides an indirect plasma treatment. In a jet configuration, the biological surface does not act as an electrode, and thus does not get affected by the charged particles in the plasma, nor does it receive an electric current. The design consists of two copper rings placed on small glass disks 2.5 cm in diameter with 3 mm perforations at the centres. The disks are then inserted in a dielectric tube and are placed at a distance of 0.5 to 1 cm apart. Helium is used as the plasma gas, and the flow rates used range from 1 to 10 L/min. The plasma is generated by applying a high voltage across the electrodes (on the order of 6 kV), and by pulsing this voltage at a very high frequency of 1-10 kHz. Since the direction of the generated electric field is parallel to the gas flow, this configuration results in a relatively long jet compared to the size of the device[44].

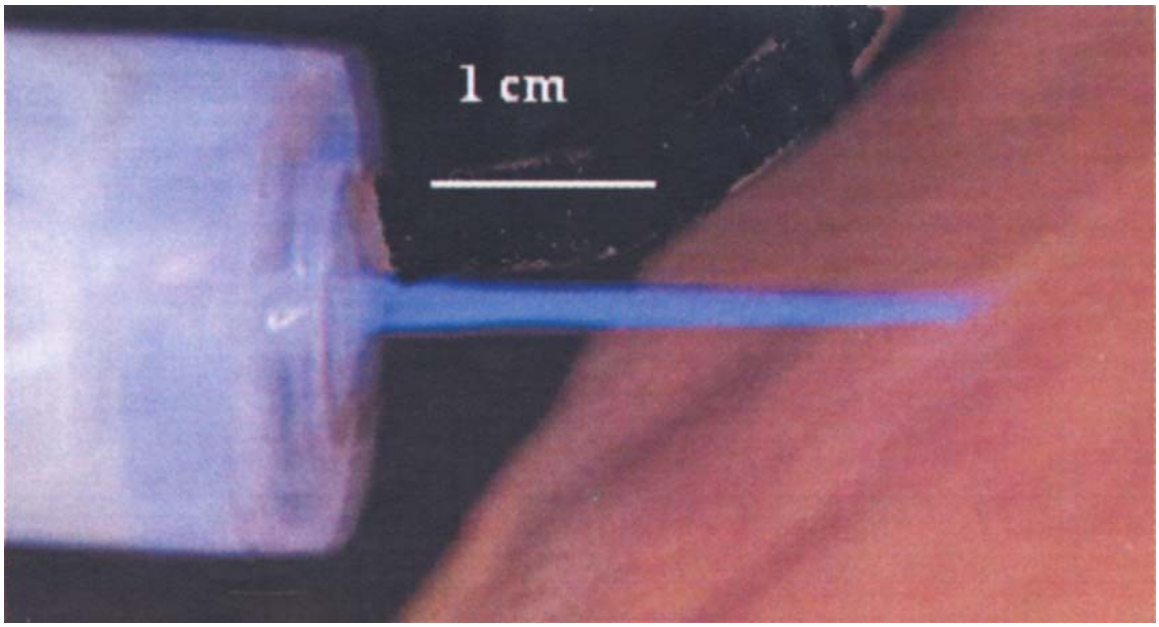

Figure 1.5: The relatively long jet of the Plasma Pencil treating a biological surface[44]

Once again, the source of reactive species in the plasma is the ambient air. However, small percentages of reactive gases were also injected into the dielectric tube in some experiments. The Plasma Pencil has mostly been used in bacteria inactivation experiments. It was shown that both gram positive and gram negative bacteria could be inactivated by the Plasma Pencil, with a higher inactivation obtained with a 0.75 vR% oxygen injection[45]. Recently, the treatment of amyloid fibrils using the Plasma Pencil was investigated. Amyloid fibrils are fibrous protein aggregates organized in a beta-sheet conformation. They are responsible for numerous neurodegenerative diseases such as Alzheimer's and Parkinson's diseases. It was demonstrated that the plasma treatment of α-synuclein protein fibrils at a voltage of 7.5 kV and a pulsed frequency of 5 kHz caused extensive breakage. This is very innovative research, since only four other methods of breaking fibrils exist, and this is the only method not based on physical mechanisms (the other methods include laser beam irradiation, ultrasonication and mechanical stirring at 1000 rpm)[46]. Although still in its early stages of research, this new application in plasma medicine is very promising and will likely be followed closely by others in the field.

1.5.4 The Atmospheric Pressure Glow Discharge torch (APGD-t)

The APGD-t generates a localized plasma jet for indirect treatment of biological surfaces. The concentric electrode configuration was adopted for the design of the APGD-t. The inner live electrode consists of a stainless steel capillary electrode with an inner diameter (ID) of 0.1778 mm and an outer diameter (OD) of 0.3556 mm. The outer electrode consists of a quartz tube, 2 mm ID and 4 mm OD, that tapers into a 500 μm nozzle with the outer surface painted in silver epoxy, which is grounded. The device is powered by an amplitude modulated RF waveform at a frequency of 13.56 Hz. The modulating waveform is a pulse at a frequency of 100 Hz, with a duty cycle of 10-50%. The novelty of the device is the capillary electrode, which allows for the direct injection of reactive species into the plasma, and thus allows for better control of the plasma chemistry[47]. Helium was used as the main plasma gas, and oxygen was used as the reactive gas injected into the capillary.

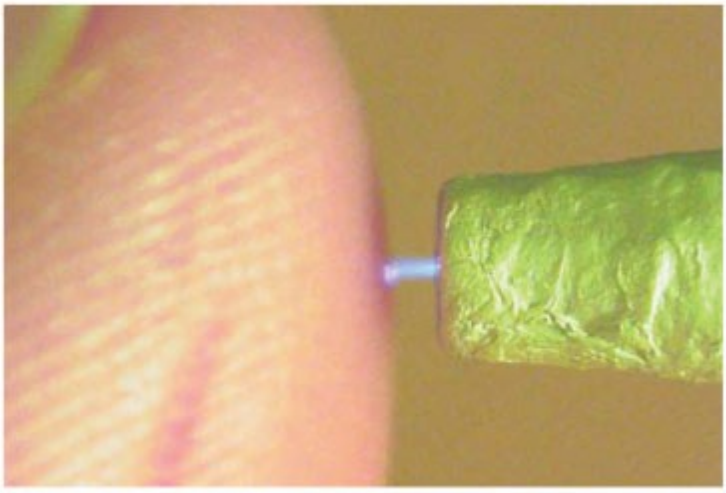

Figure 1.6: The atmospheric pressure plasma torch applied to a human thumb[48]

The APGD-t has been extensively characterized, with a focus on impedance matching, phase angle measurement calibration, and power dissipation calculation[47, 49]. Typical voltages and currents across the device are 405 V peak-to-zero and 0.46 A peak-to-zero, which, taking into account the phase angle, corresponds to a power dissipation in the plasma of approximately 1 W at a 10% duty cycle. As with the other jet configurations presented, air entrainment is a source of reactive species. However, it was shown that

injecting O_2 into the main plasma gas resulted in a constriction of the plasma jet, whereas when O_2 was injected into the capillary, the plasma jet was unaffected. Axial spectroscopy measurements of the plasma also demonstrated that the generated RS, specifically atomic O, were transported further downstream with O_2 injection in the capillary. This design therefore presents an advantage for the delivery of short lived species.

The primary focus of studies involving the APGD-t was on plasma interactions with mammalian cells. The types of interactions studied included cell detachment, cell permeabilization, and damage of naked DNA caused by plasma interactions. It was demonstrated that treating HepG2 cancer cells with the APGD-t at 10% duty cycle resulted in cell detachment, with the detached cells reattaching within 15 minutes onto a new plate. The detached cells also showed evidence of permeabilization with propidium iodine (PI) fluorescent dye, indicating damage to the membrane. Nevertheless, an MTT assay of the re-attached cells demonstrated their continued proliferation. The authors therefore proposed a non-lethal lipid peroxidation as a mechanism for the permeabilization of the membrane[50]. In another study, dextrans of increasing hydrodynamic radii were used to determine the approximate size of the pores on the cell membrane created by the plasma treatment. In HeLa cells, it was found that dextrans with radii of up to 4.8 nm were taken up by the cells, whereas dextrans of radius 6.5 nm were unable to diffuse through. It was then demonstrated that under mild operating conditions, there was no damage to naked DNA in culture medium, specifically to hrGFP-II-1 plasmids. These plasmids were then shown to be successfully transfected in the plasma, with a maximum local efficiency of 35%[51].

1.6 Biological NO and ROS

As seen in section 1.4, NO and ROS produced in NAPP have the most important roles during plasma interactions with both eukaryotic and prokaryotic cells. This is not a surprising result, as these molecules are known in the field of biomedicine as signalling molecules which are produced in mammalian cells and have important roles in almost all cellular functions. Both hold very important roles in non-specific host immune response[52], and are crucial for the eventual clearance of *Leishmania* parasites during

CL. In order to understand how externally, or exogenously, produced NO and ROS affect prokaryotic and eukaryotic cells, it is necessary to understand how and under what conditions endogenous NO and ROS are synthesized and how they subsequently affect the biological functions of the host. This review focuses on the immune functions of NO and ROS in macrophages and other phagocytes, given that these functions are disrupted by *Leishmania* infections.

1.6.1 Endogenous production of NO

As is the case with many biologically active components in cells, the generation of NO requires the presence of a specific type of enzyme, the NO synthases (NOS), along with specific reactants, namely the amino acid arginine and oxygen, in order to be generated. NOS catalyses the five-electron oxidation of the guianidino nitrogen of arginine, producing NO along with citrulline. There are three types of NOS, two constitutive and one inducible. A constitutive enzyme is an enzyme which is produced in all physiological conditions, whereas an inducible enzyme is only expressed under stimuli. The two constitutive NOS are ncNOS and ecNOS, named as such because they were first cloned from neuronal and endothelium cells, respectively. The inducible NOS is known as iNOS. The two constitutive enzymes, which are always present, are regulated by intracellular levels of calcium through the calcium binding messenger protein calmodulin. When activated, they produce short pulses of NO in the nmol/L range. The NO produced in this case acts as a regulator of very rapid events, such as vasorelaxation and neurotransmission. The inducible NOS, on the other hand, is not activated by calcium, but rather is transcriptionally regulated. Depending on the cell, iNOS can be induced by various external stimuli. iNOS continuously produces NO for longer periods of time at concentrations in the μmol/L range. In this case, NO is generated because of its cytotoxic properties as part of the host immune response[2]. Since NO is a radical, it will react quickly with other molecules with unpaired electrons. However, this is not the case for most biological molecules, and thus NO is cell permeable and can diffuse over long lengths *in vivo* without reacting. NO is often said to have a short half-life, but from the reaction kinetics of NO in solution, it can be seen that the half-life of NO is reversibly proportional to its concentration. Thus, at physiologically relevant concentrations (from 5 nmol/L to 4μmol/L) this half-life is on the order of 1 second[53]. In mammals, the main

mechanism of NO removal is through the circulatory system, where it reacts with oxyhemoglobin to form nitrate and methemoglobin. Although NO has a relatively long lifetime *in vivo* and readily diffuses through cells, the high rate of collisions restricts the total distance travelled by NO to within a few cells of where it is produced[52].

1.6.2 Endogenous production of ROS

A wide range of ROS are found in cellular environments, including superoxide ($O_2^{\bullet -}$) hydroxyl (OH•) singlet oxygen (Δ^1O_2), hydrogen peroxide (H_2O_2) hypochlorous acid (HOCl) and ozone (O_3). Although some ROS are produced non-enzymatically as by-products of other cellular reactions (e.g. aerobic respiration), there are intentional enzymatic mechanisms by which cells produce ROS[54]. Enzymatic ROS production involves the oxidation of the reduced form of nicotinamide adenine dinucleotide phosphate (NADPH). In phagocytes, this is catalysed by an enzyme complex named the NADPH oxidase. This complex is made up of several subunits: a catalytic subunit (gp91phox) and several regulatory subunits (p22phox, p47phox, p40phos and p67phox). Seven homologs of the catalytic subunit gp91phox, or NADPH oxidase 2 (NOX2) exist, and these are responsible for ROS generation in different cell types using various regulatory mechanisms. Together, they form the NOX family of enzymes which is largely responsible for ROS production in all tissue[55]. The NADPH oxidases are transmembrane complexes, and in phagocytes they can form at both the outer cell wall and intracellular membranes. Complex formation involves a specific series of steps in which different subunits assemble and activate. Once active, the complex generates superoxide by transferring an electron from NADPH in the cytoplasm to the an oxygen molecule either in the extracellular environment, or inside the vacuolar space (e.g. the phagosome)[54]. Of the ROS given above, superoxide is the least reactive. However, the presence of other phagocytic enzymes and molecules lead to the formation of much more reactive ROS. Superoxide dimutase (SOD) catalyses the reduction of superoxide to hydrogen peroxide. Superoxide and hydrogen peroxide can react to form the hydroxyl radical when catalysed by iron. Myeloperoxidase (MPO) catalyses the reaction between hydrogen peroxide and chloride that forms hypochlorous acid, who's oxidated form further reacts with hydrogen peroxide to form singlet oxygen. Ozone is formed by the reaction between superoxide and hydrogen peroxide, catalysed by antibodies of any

specificity[56]. This consumption of oxygen followed by the production of numerous types of ROS is called the respiratory burst. It occurs primarily in phagocytic cells as part of the innate immune response, but also has various roles in other cell types, for example in cell signalling, gene expression, proliferation, apoptosis and angiogenesis[54]. The cell membrane permeability of different ROS vary, superoxide having lower permeability than hydrogen peroxide. This, combined with their reactivity and cellular environment, defines their diffusion distance, reviewed for various species by Winterbourn[57].

1.6.3 Biological functions of NO and ROS in the immune system

The production of NO and ROS is part of the antimicrobial defence system of phagocytes. They are induced by cytokines, microbial products, and phagocytosis, which all indicate the presence of a pathogen. Although ROS production can begin quickly after pathogen presence is recognized, NO production is slower since iNOS is transcriptionally regulated and must first be synthetized. Both have diverse antimicrobial effects and can act separately as well as synergistically. Molecular targets of ROS damage include DNA, proteins, and membrane lipids. Microbicidal NO action includes inhibition of metalloproteins required for DNA replication, bacterial replication inhibition, and ribonucleotide reductase inhibition. Peroxynitrite ($ONOO^-$), formed by the rapid and irreversible reaction of NO with superoxide, also contributes to phagocyte antimicrobial activity. The reaction rates of superoxide with these enzymes and with NO are about equivalent, meaning that peroxynitrite is only produced when the concentration of NO surpasses that of superoxide dismutase[53]. Thus, an increased production of either NO or superoxide can result in a substantial increase in peroxynitrite production.

There are a large number of biological functions of NO and ROS in the immune system outside of antimicrobial activity. NO produced by macrophages has been associated with cytokine and chemokine regulation (both up and down), differentiation and inhibition of T-cells, pro and anti-inflammatory activity, and immune cell proliferation and apoptosis[58]. Likewise, ROS were shown to affect both cell proliferation and apoptosis[59]. The reason these molecules have been attributed to seemingly opposite effects can be explained by the wide range of oxidative stress in cellular environments. Low oxidative stress will tend to control normal cell function and promote proliferation,

whereas mid-range oxidative stress will induce cell activation, pro-inflammatory responses, apoptosis and antimicrobial activity. Both these types of responses are due to NO and ROS modulation of cell signalling, also known as redox signalling. At higher levels of oxidative stress, DNA and other essential biomolecules will be irreparably damaged, and necrosis will occur[60].

An excellent (and relevant) example of the use of redox signalling is during wound healing, shown in Figure 1.7: The production of NO during the different stages of wound healing[61]. When a wound is formed, NO is abundantly produced by inflammatory cells, especially macrophages, during the earliest stage i.e. inflammation. Skin cells contribute to the continued production over the later stages, proliferation and regeneration, but the overall NO concentration decreases over time, as the wound heals. The role of NO in the early stages of wound healing is most likely to protect against infection (hence the cytotoxic levels of NO produced), and the proposed role of NO in the later stages is the promotion of collagen formation[61].

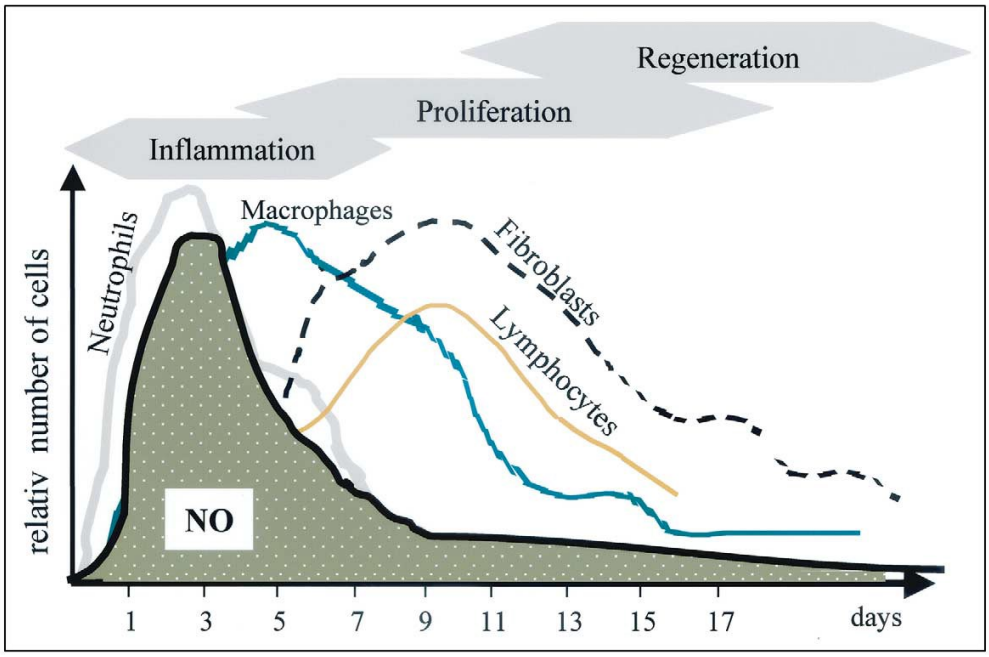

Figure 1.7: The production of NO during the different stages of wound healing[61]

1.7 Cutaneous Leishmaniasis

1.7.1 Overview

Leishmaniasis is a group of diseases caused by parasites of the genus *Leishmania*. Leishmaniasis is commonly referred to as a neglected disease, since it is endemic to tropical and subtropical countries and affects people of lower socioeconomic status. Yet 350 million people worldwide are considered at risk of infection, and 2 million new cases are reported each year[62]. Endemic transmission of leishmaniasis has been reported in 98 countries and 3 territories over 5 continents, making leishmaniasis a global health issue[63]. There are four clinical manifestations of leishmaniasis: (1) localized CL, (2) diffuse CL, (3) mucosal leishmaniasis and (4) visceral leishmaniasis[64]. The different manifestations are caused by different species of *Leishmania*, which are also classified by subgenus (*Leishmania* and *Viannia*) and geographical location (Old World and New World). The *Leishmania* species which cause infection in humans, along with their manifestation and geographical location, are given in Table 1.1 below. *Leishmania* species are predominantly transmitted to humans and other mammals by sandflies, specifically by the genus *Phlebotomus* in the Old World and *Lutzomyia* in the New World**[64]**.

Table 1.1: Leishmania species which cause human disease. Adapted from Reithinger et al. [64]

	Manifestation	**Geographical distribution**
New World		
L. Viannia braziliensis	Local cutaneous, mucosal	South America, parts of central America, Mexico
L. Viannia panamensis	Local cutaneous, mucosal	Northern South Americal and southern Central America
L. Viannia peruviana	Local cutaneous	Peru
L. Viannia guyanensis	Local cutaneous	South America
L. Viannia lainsoni	Local cutaneous	South America
L. Viannia colombiensis	Local cutaneous	Northern South America
L. Leishmania amazonensis	Local and diffuse cutaneous	South America
L. Leishmania mexicana	Local and diffuse cutaneous	Central America, Mexico, USA

L. Leishmania pifanoi	Local cutaneous	South America
L. Leishmania venezuelensis	Local cutaneous	Northern South America
L. Leishmania garnhami	Local cutaneous	South America
Old World		
L. Leishmania aethiopica	Local and diffuse cutaneous	Ethiopia, Kenya
L. Leishmania killicki	Local cutaneous	North Africa
L. Leishmania major	Local cutaneous	Central Asia, north Africa, middle east, East Africa
L. Leishmania tropica	Local cutaneous	Central Asia, middle east, parts of North Africa, southern Asia
L. Leishmania donovani	Local cutaneous, visceral	Africa, central Asia, southeast Asia
New and Old World		
L. Leishmania infantum	Local cutaneous, visceral	Europe, north Africa, Central America, South America

1.7.2 Life cycle of *Leishmania* species

The transmission of *Leishmania* between insect vectors and mammalian hosts is a crucial part of its life cycle, shown in Figure 1.8. When the sandfly takes a blood meal, it regurgitates *Leishmania* promastigotes, which are the mobile form of the parasites. This form is specialized for resistance to the complement system, a part of the innate immune response, and for enhanced infectivity[9]. Although the promastigotes initially infect numerous types of phagocytic cells, the long term cellular hosts of *Leishmania* are macrophages[65]. The promastigotes are internalized by phagocytosis, and thus initially reside in an intracellular vesicle named the phagosome. During normal phagocytosis, the phagosome containing the internalized pathogen binds with a lysosome to form the phagolysosome, where the pathogen is digested by the lysosome's hydrolic enzymes. However, this process is modulated by *Leishmania* species during infection. After promastigote internalization, the phagosome will fuse with different endocytic organelles (e.g. lysosomes and late endosomes) and mature to form a "parasitophorous vacuole". This process occurs in parallel with the transformation of promastigotes to amastigotes, the non-mobile form of the parasite[66]. The amastigote is specialized for survival inside

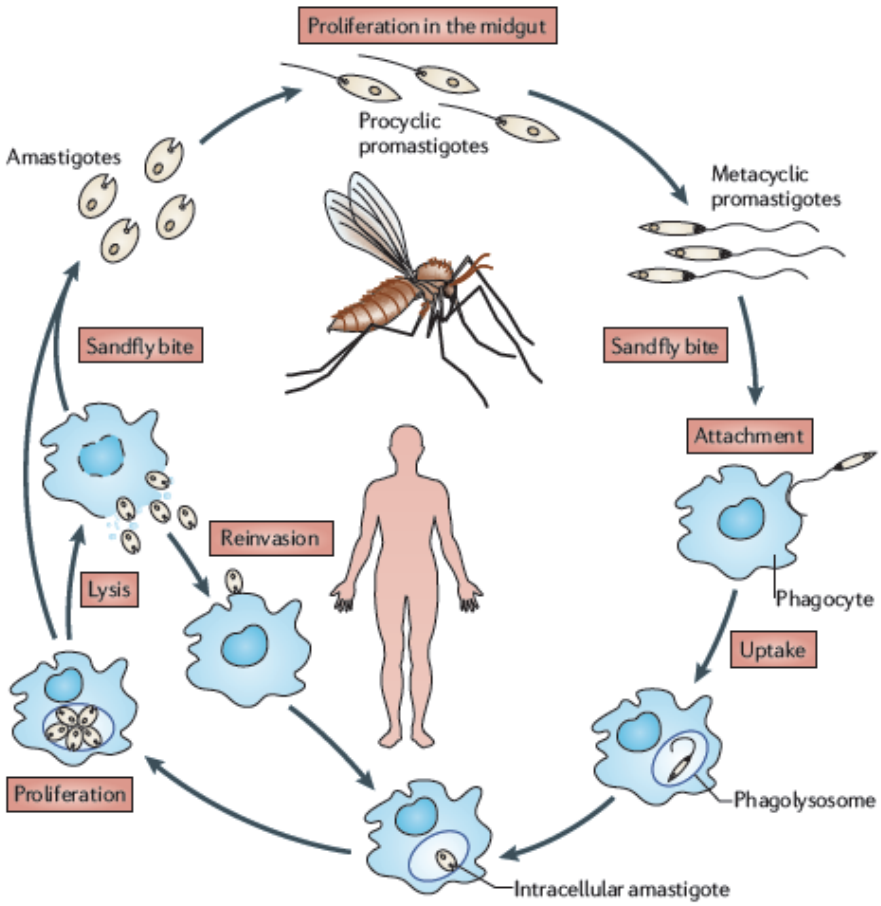

Figure 1.8: Life cycle of *Leishmania species* [65]

the parasitophorous vacuole, and will proliferate in this environment until the large number of amastigotes causes the host cell to burst.

The amastigotes will then be phagocytosed by macrophages in the surrounding environment, thus infecting new cells. When a sandfly takes a blood meal from an infected mammal, these infected macrophages are taken up along with other free amastigotes in the blood. The parasites will reside inside the digestive track of the sandfly, where they eventually transform into infectious metacyclic promastigotes and migrate to the stomodeal valve, the ideal location for inoculation of the next mammalian host[66].

1.7.3 Clinical manifestation of CL

When the species of *Leishmania* regurgitated into the skin is dermotropic, they will remain in the skin at the site of the sandfly bite, and CL will develop[67]. After a species dependant incubation period, the skin will develop an erythematous papule, or reddened solid elevation smaller than 0.5 cm. This papule will then grow to become a nodule, or elevation larger than 0.5 cm. The nodule will begin to ulcerate, eventually forming the lesion associated with CL. The lesion can evolve into a wide variety of the clinical forms[68]. It is possible for the lesion to heal spontaneously after a period ranging from 2-15 months depending on the *Leishmania* species and host immune response. These cases are referred to as acute CL. Spontaneous healing of the disease provides long term immunity against re-infection. Once the infection is cleared, the lesion will be replaced with a permanent scar, which depending on the size and location can be disfiguring and psychologically damaging for the individual. Several non-healing cases of the disease also exist, including chronic CL (non-healing wounds), leishmaniasis recidivans (new papules appearing around a healed lesion), diffuse CL (when the papules spread to the face or the entire body), and the potentially fatal mucosal leishmaniasis (CL that spreads to mucous tissue, thus affecting the nasal passage, lips, cheeks, soft palate etc.) [64, 68]. The exact causes for these chronic forms of the disease are not known, although diffuse cutaneous and mucosal leishmaniasis are only caused by certain species of *Leishmania* (refer to Table 1.1). They are also extremely difficult to treat with traditional methods.

1.7.4 Treatments

After diagnosis, CL is monitored and treated to prevent further scarring and to prevent chronic manifestations of the disease. In its 2010 technical report on the control of leishmaniasis, the World Health Organization (WHO) provides updated treatment options for CL. Traditional “antileishmanial medicines” include pentavalent antimonials, amphotericin B deoxycholate, paromomycin, pentamidine isethionate and miltefosine. These are typically used as aggressive systemic therapies administered by painful intravenous or intramuscular injections. They are expensive drugs which have severe adverse side effects, and therefore their use is only suggested when the CL infection is severe (more than four lesions), is disfiguring or disabling, or has evolved into a non-healing form. For smaller, uncomplicated cases of CL, WHO suggest local therapies such

as intralesional pentavalent antimonials, topical paromomycin ointments, thermotherapy (heating lesion area to 50°C) and cryotherapy with liquid nitrogen[62]. These local therapies can cause pain at the lesion site, and physical treatments are expensive due to equipment costs.

1.7.5 Subversion of host immune response

In order to survive within mammalian hosts, *Leishmania* species must evade the innate and adaptive immune response. Most importantly, they must alter the normal response of macrophages to extra and intracellular pathogens by keeping it in an inactive state[64]. Leishmaniasis research often focuses on the interaction between the parasite and the macrophage, since understanding the mechanisms of macrophage subversion is essential for understanding the disease and developing potential treatments. An important aspect of this macrophage subversion is blocking the production of cytotoxic ROS and NO, as well as resisting their toxic effects. This will be the focus of the following review, given that the treatment potential of atmospheric plasmas for leishmaniasis derives from their ability to produce ROS and NO.

Manipulation of the macrophage immune response begins with the initial interaction with the parasite. As previously stated, *Leishmania* promastigotes are able to resist the complement system, an innate immune response in which the membrane attack complex (MAC) is formed on the cell membrane of a pathogen, causing cell lysis. The *Leishmania* surface protein gp63 is responsible for the cleavage of one of the complement components of the MAC called C3 into C3b and subsequently into C3bi. This both (1) inhibits other complement components from attaching to the parasite membrane and (2) promotes the attachment of the parasite to the complement receptor 3 (CR3) rather than CR1 on the surface of the macrophage. The latter reduces the oxidative burst associated with phagocytosis by the macrophage[9]. Inside the macrophage, *Leishmania* promastigotes reside inside phagosomes, and later inside the parasitophorous vacuoles (altered phagolysosome) as amastigotes. As previously stated, this transition is modulated by the parasite in order to avoid digestion by the macrophage. Several studies demonstrate a modulatory effect of phagosome maturation by the surface molecule LPG,

one of which demonstrating that delayed maturation of the phagosome contributes to promastigote survival[69].

A large part of the *Leishmania* parasite's survival strategy is the inhibition of NO production, which it achieves through the control of iNOS expression. Several signalling pathways involved in iNOS expression are affected by *Leishmania* infections. These include the Janus Kinase (JAK) and the Signal Transducer and Activator of Transcription (STAT) pathway named the JAK-STAT pathway[70], the mitogen activated protein kinases (MAPKs)[71] signalling cascade and downstream transcription factors activator protein 1 (AP-1) and nuclear factor kappa-light-chain-enhancer of activated B cells (NF-κB). One of the principal mechanisms proposed for the control of these pathways is the cleavage of protein tyrosine phosphatases (PTPs) by gp63. In cell signalling, signal cascades are controlled by kinases and phosphatases. The kinase is responsible for activating a signalling molecule by phosphorylation and the phosphatase deactivates it by dephosphorylation. A signal is therefore typically transmitted from the cell membrane to the nucleus by a series of kinases (e.g. the MAPK signalling cascade), shown in Figure 1.9. A delicate balance between the activation state of kinases and phosphatases must therefore exist in the cell. *Leishmania* parasites disrupt this balance by activating certain PTPs through cleavage, which then dephosphorylate important signalling molecules. Gomez *et al.* demonstrated that PTPs activated by gp63 induced cleavage include SHP-1, PTP1B, and TCPTP[72].

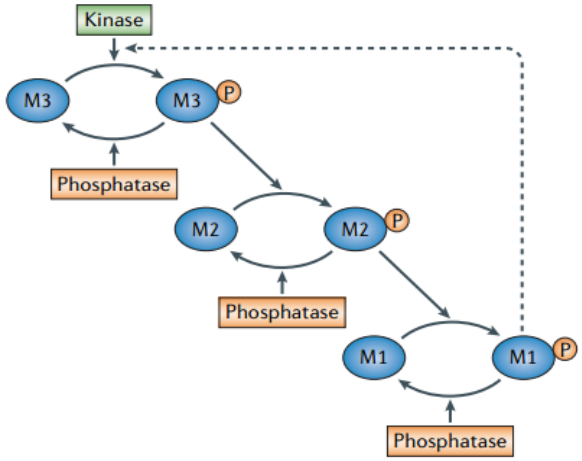

Figure 1.9: Signalling cascade mediated by kinases and phosphatases[73]

The macrophages' ability to eventually clear *Leishmania* parasites is dependent on the induction of a Th1 immune response by $CD4^+$ (or helper) T cells. There are two types of helper T cells, which can be distinguished by the types of cytokines they produce. The cytokines produced by these cells will then determine the type of immune response mounted by the immune system. Th1 cells produce pro-inflammatory cytokines such as Interferon-γ (IFN-γ) which activate macrophages and other phagocytes to kill intracellular pathogens. Th2 cells produce cytokines such as Interleukin-4 (IL-4) which promote an antibody response to attack extracellular pathogens. The differentiation of helper T-cells is mediated by cytokines. IL-12 induces a Th1 response and IL-4 induces a Th2 response. Mouse strains which exhibit a Th1 response are typically resistant to chronic CL infections, whereas strains which exhibit a Th2 response will develop non-healing lesions. This typically also seen in human CL, where self-healing patients will exhibit a Th1 response and chronic sufferers will exhibit a Th2 response[74]. It is important to remember not to generalize to all CL cases, given the large variety of *Leishmania* strains and of possible immune responses profiles of the infected hosts.

Chapter 2 : Project Objective

The primary goal of this thesis was to investigate the potential of plasma treatments as a therapy for cutaneous leishmaniasis. The specific objectives of the project were:

- To design a NAPP device capable of producing RS including NO and ROS
- To perform a preliminary assessment of the plasma device using electrical and emission spectroscopy measurements
- To perform a preliminary study of *in vitro* plasma treatments of macrophages to determine their effects on signalling and function
- To perform a preliminary study of *in vitro* plasma treatments of *Leishmania* species to investigate their cytotoxic effects on this pathogen
- To perform a preliminary study of *in vivo* plasma treatments using a mouse model for CL to determine their effect on lesion development

Chapter 3 : Materials and Methods

3.1 Device & means of characterization

3.1.1 APGD-j

The Atmospheric Pressure Glow Discharge jet (APGD-j) device was used in this investigation. It is a second generation device, the first generation being the Atmospheric Pressure Glow Discharge torch (APGD-t). The design and characterization of the APGD-t have previously been described[47]. Although the APGD-j has been scaled up from its previous incarnation, most of the design characteristics remain the same. A schematic of the APGD-j can be seen in Figure 3.1. Namely, the device consists of (1) a concentric cylindrical geometry featuring a capillary electrode at the centre, (2) a tapered nozzle to induce high gas velocities, (3) two gas lines, one for reactive gas injection into the capillary electrode and one for the plasma forming gas injection between the two electrodes and (4) amplitude modulated RF power supplied to the capillary electrode. The device has been scaled up in order to increase the treatment area, as well as to facilitate the impedance matching of the circuit. The APDG-j now consists of a grounded outer electrode made of stainless steel and an adjustable brass capillary inner electrode. The inner electrode is held in place by a stainless steel compression fitting inserted into a ceramic insulator. An O-ring is positioned between the grounded electrode and the ceramic piece and is compressed by an aluminum sleeve which acts as an RF shield. Helium gas was used as the plasma forming gas, and nitrogen and oxygen were used as reactive gases. Helium flow rates of 1-6 standard litres per minute (slm) and reactive gas flowrates of 10 standard cubic centimeters (sccm) were employed.

The power applied to the device consists of an RF signal which is square-wave amplitude modulated at 500 Hz, with a duty cycle of 5-15%. Both the carrier and modulation frequencies are provided by a function generator (Tektronix #AFG3102). The signal is amplified by an RF amplifier (Ophir #5084). The matching network consists of a single inductor placed in series between the amplifier and the torch. Initially, a 1.3 μH inductor was chosen by estimating the inductance required for circuit matching at 13.56 mHz (an

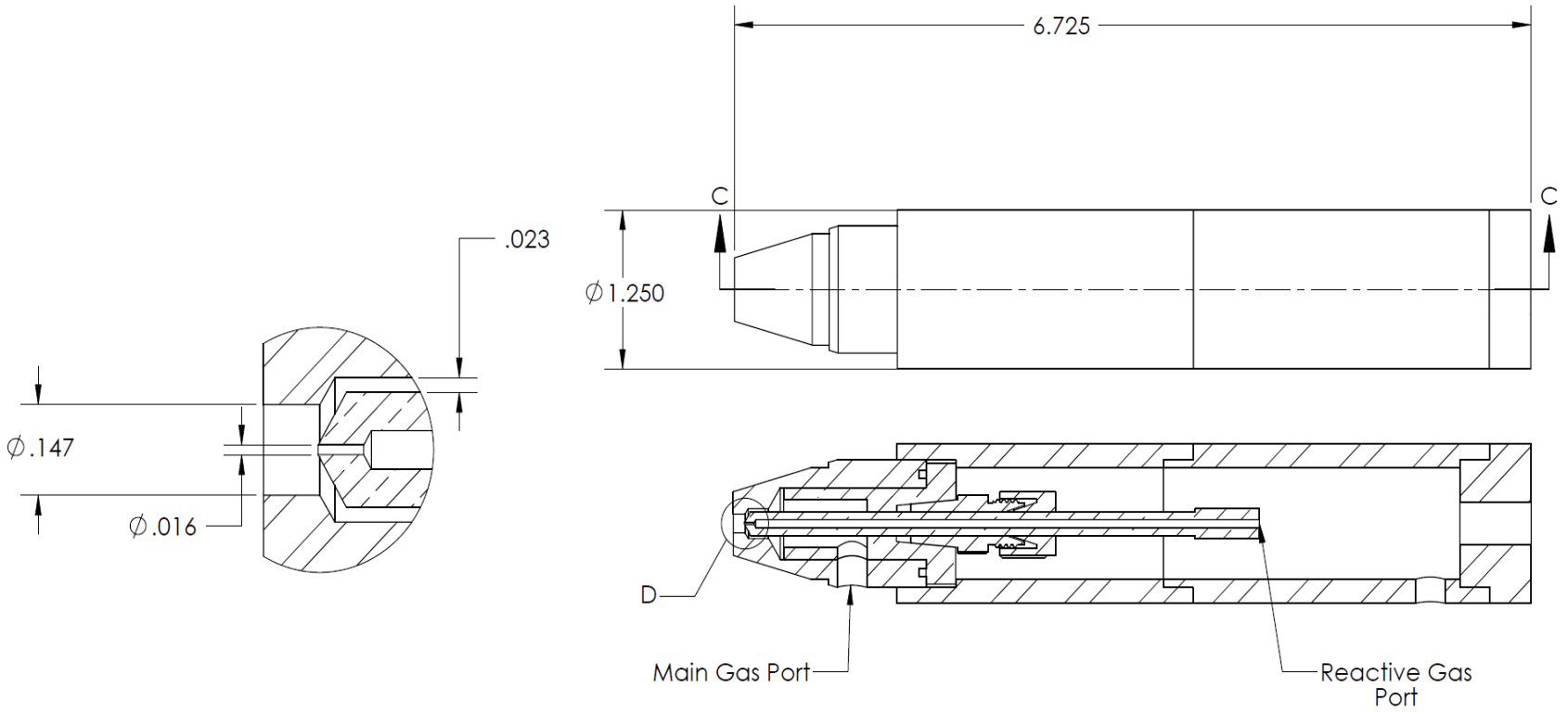

Figure 3.1: Total and cross-sectional views of the APGD-j, along with a close-up of the plasma forming region. Dimensions are in inches.

industry standard). The excitation frequency was subsequently tuned to near-resonance, found at 18 MHz. Electrical measurements of the plasma device were taken using a voltage probe (Tektronix P5100), current probe (Tektronix CT2) and oscilloscope (Tektronix TDS2012B). The breakdown and sustaining voltage obtained with this circuit are 400 V and 200 V peak-to-zero, respectively, and the sustaining current is 2 A. The carrier and modulation frequencies as well as the plasma forming and reactive gas flowrates are controlled using an NI-LabVIEW^{TM} interface.

3.1.2 Optical Emission Spectroscopy (OES)

The broadband UV-visible spectrum emitted from the plasma was recorded using a spectrometer (Ocean Optics #USB2000) and a UV/NIR range fibre optic patch cable (Thorlabs #M22L01). The fibre was mounted face on, directly at the exit of the plasma in order to capture the line-of-sight emission. An integration time of 150 ms was used to acquire the entire spectrum, and an integration time of 2000 ms was used to acquire the UV spectrum.

3.1.3 Nitrite (NO_2^-) assay

The concentration of nitrite in solution after plasma treatment was measured using the Griess reagent system. The reagent consists of a mixture of sulfanilic acid and N-(-Naphthyl)ethylenediamine). Sulfanilic acid will react with nitrite to form diazonium salt, which will then react with N-(-Naphthyl)ethylenediamine) to form a pink azo compound. The concentration of this compound can be quantified in a microplate spectrophotometer by measuring absorbance at around 540 nm.

3.2 *in vitro* investigation

3.2.1 Cell culture

The bone-marrow derived murine macrophage cell line B10R (Obtained from Dr. Danuta Radzioch, McGill University) was cultured in Dulbeco's Modified Eagle Serum (DMEM) (Wisent) supplemented with 10% Fetal Bovine Serum (FBS) (v/v) (Gibco), streptomycin (100 µg/ml), penicillin (100 U/ml), and 2 mM L-glutamine at 37°C and 5% CO_2. An *L. major* strain stably transfected with the luciferase reporter gene (Lm-LUC)[75] was cultured in promastigote form in Schneider's Drosophila Medium (SDM)

supplemented with 10% FBS (v/v) and hemin (5 mg/mL) in a closed environment at 25°C.

3.2.2 Plasma treatment of macrophages

Twenty four hours before treatment, 0.25×10^6 macrophages were plated per well of a standard 12 well plate, giving 0.5×10^6 macrophages on the day of the expeirment. Immediately before treatment, the cells were washed in phosphate buffered saline (PBS) and the cell culture media was replaced with 1 mL phenol red-free Rosewell Park Memorial Institute Medium (RPMI) per well. Two types of plasma treatments were employed in this study: direct and indirect. For direct plasma treatments, the RPMI above the plated macrophages was treated directly with the APGD-j. For indirect plasma treatments, 1mL RPMI in a separate 12 well plate was treated and then transferred immediately onto the cells. In both cases, the APGD-j was placed approximately 3 mm above the surface of the RPMI. A duty cycle of 10% and a He flow rate of 2 slm were used for all plasma treatments. A negative control of 2 slm He gas only was used for all experiments. The length of the treatment (1-10 min) and post-treatment incubation time (15 min to 2 h) varied depending on post-treatment analysis. 100 mM of LPS was used as a positive control.

3.2.3 Western Blot

Following a defined incubation period, the treated cells were washed in PSB and lysed in Western Blot lysis buffer (PBS, 1% Igepal, 2% Glycerol, 0.02% inhibitor cocktail, 0.01% of 200 mM Na_3VO_4 solution, 0.005% of 100 mM NaF solution). The wells were then scrapped and the liquid was transferred to microcentrifuge tubes. The tubes were centrifuged at 13 000 rpm for 15 min at 4°C, and the supernatants were transferred to new tubes and kept on ice. The proteins were dosed using the Bradford reagent (Biorad) and 15-30 µg of protein from each sample were denatured with sample loading buffer (SLB) (50 mM Tris-HCl pH 6.8, 2% SDS, 10% glycerol, 1% 2-mercaptoethanol, 12.5 mM EDTA, 0.02% bromophenol blue) at 90°C for 3 minutes. The samples were then loaded onto a 10% SDS-PAGE. After gel electrophoresis, the standard electroblotting procedure was used to transfer the proteins onto a polyvinylidene difluorise (PVDF) membrane. The membrane was blocked with 5% Bovine Serum Albumin (BSA) (w/v) in

TBS-T for 30 minutes at room temperature, then soaked in primary antibody solution for 1-3 hours at room temperature, or overnight at 4°C, depending on the antibody. These include phospho p38, p38, phospho JNK, JNK, phospho ERK, ERK and actin (Cell Signalling). Anti-mouse or anti-rabbit antibodies conjugated to horse-radish peroxidise (HRP) (GE Healthcare) were used as secondary antibodies. The membranes were exposed to the chemiluminescent substrate (Pierce) for 1 min, then to photographic film.

3.2.4 Electrophoretic Mobility Shift Assay (EMSA)

Following a defined incubation period, the treated cells were washed in PSB and lysed in buffer A (10 mM HEPES (pH 7.9), 10 mM KCl, 1.0 mM DTT, and 0.5 mM PMSF), which was transferred to microcentrifuge tubes and stored on ice. After a 15 min incubation, 10% igepal (v/v) was added to each sample, which were centrifuged at 13 000 rpm for 1 min at 4°C. The pellets were then gently resuspended in buffer B (20 mM HEPES (pH 7.9), 0.4 M NaCl, 1 mM EDTA, 1 mM EGTA, 1 mM DTT, and 1 mM PMSF), rocked for 15 minutes at 4°C and centrifuged at 13 000 rpm for 15 min at 4°C. The supernatants, which contained the nuclear proteins, were transferred to new tubes and kept on ice. The proteins were dosed using the Bradford reagent (Biorad) and 6 μg of nuclear proteins were incubated for 20 min at room temperature in binding buffer (100 mM HEPES (pH 7.9), 40% glycerol, 10% Ficoll, 250 mM KCl, 10 mM DTT, 5 mM EDTA, and 250 mM NaCl), poly(dI-dC) and nuclease-free BSA (fraction V; Sigma-Aldrich) containing 1.0 ng of dsDNA oligonucleotide radiolabelled with γ-32P poly(Glu4Tyr) peptides (Sigma-Aldrich). The dsDNA oligonucleotides were NF-κB (5′-AGTTGAGGGGACTTTCCCAGGC-3′), AP-1 (5'-AGCTCGCGTGACTCAGCTG-3') and SP-1 (5′-ATTCGATCGGGGCGGGGCGAGC-3′) (Santa Cruz) as non-specific control. Following 20 min of incubation, the reaction was terminated using 0.2 M EDTA and the samples were loaded onto a 4% (w/v) polyacrylamide gels containing 50 mM Tris-HCl (pH 8.5), 200 mM glycine, and 1 mM EDTA. After electrophoresis, the gel was dried and exposed to autoradiography film.

3.2.5 Quantitative Reverse Transcription Polymerase Chain Reaction (qRT-PCR)

After an 8 hour incubation period, the cells were washed with PBS and the total RNA was extracted using TRIzol reagent (Invitrogen) according to manufacturer's protocol. DNase I (Promega) was used to clear all possible genomic DNA contamination. After RNA quality and quantity assessment using a microvolume spectrophotometre (NanoDrop), 1 μg of RNA was used for qRT-PCR using RT^2 Profiler PCR Array System for mouse innate and adaptive immune responses (SABiosciences) according to the manufacturer's protocol. Results were analyzed using the ΔΔCt method.

3.2.6 Plasma treatment of *L. major* promastigotes

Immediately before treatment, the cells were centrifuged at 2000 rpm for 5 minutes, washed in PBS, centrifuged again at 2000 rpm for 5 minutes and resuspended in phenol red-free Rosewell Park Memorial Institute Medium (RPMI) to give 0.2×10^6 parasites/μL. Both direct and indirect plasma treatments were tested. For direct plasma treatments, 400 μL of the RPMI parasite suspension was treated directly with the APGD-j. For indirect plasma treatments, 400 μL of RPMI was treated in a separate 24 well plate and immediately used to resuspend the cells. In both cases, the APGD-j was placed approximately 3 mm above the surface of the RPMI. A duty cycle of 10% and a He flow rate of 3 slm were used for all plasma treatments. A negative control of 3 slm He gas only was used for all experiments. The length of APGD-j treatments was 5 minutes, and the incubation was overnight at 25°C. 1 mM of hydrogen peroxide (H_2O_2) was used as a positive control.

3.2.7 Parasite viability assays

Following the overnight incubation, double distilled H_2O was used to equalize the volumes of all samples (to compensate for evaporation during treatment). Flow cytometry and colorimetry were used to assess cell wall integrity and cell metabolic activity, respectively. One aliquot of the parasite suspension was stained with propidium iodide (PI) and dye exclusion was performed using the FACSCanto II (BD Biosciences). Results were analysed using the FlowJo software package. A second aliquot of the parasite suspension was analysed using the XTT assay. The reagent (1.34 mM 2,3-Bis(2-

methoxy-4-nitro-5-sulfophenyl)-2H-tetrazolium-5-carboxanilide inner salt (XTT salt) and 24.5 μM of N-methyl dibenzopyrazine methyl sulfate (PMS)) was added 1:1 to the suspension, and incubated between 30 and 60 min. The concentration of the bright orange formazan (produced by the reduction of XTT by cell metabolic activity) was quantified in a microplate spectrophotometer by measuring absorbance at 540/630 nm.

3.2.8 *in vitro* Infection and luciferase assay

B10R macrophages were plated in a standard 24 well plate to obtain 0.25×10^6 macrophages per well on the day of infection. One aliquot of each parasite suspension containing 5×10^6 promastigotes before treatment was used for infection, giving an ideal ratio of 20:1. The macrophages were infected for 6 hours at 37°C and 5% CO_2, washed three times with PBS to remove non-internalized promastigotes and incubated overnight at 37°C and 5% CO_2. Half the cells were collected immediately after the initial 6 hour infection, and the other half after the overnight incubation following infection. The lysing solution was 1:5 diluted Firefly lysis buffer (Biotium). The proteins were dosed using the Bradford reagent (Biorad). Amastigote concentration was determined using the luciferase assay detection kit (Promega) according to the manufacturer's protocol. Briefly, 45μL of luciferin reagent was added to 5 μL of lysate, and the emitted light is quantified by a microplate luminometer.

3.3 *in vivo* investigation

3.3.1 *in vivo* infection and treatment of mice

6-8 week old female BALB/c mice (Charles River Laboratories) were housed in the Duff Medical building animal facility. Experiments were performed in accordance with guidelines of the Canadian Council on Animal Care, as approved by the Animal Care Committee of McGill University. Sterile PBS containing 5×10^6 luciferase expressing *L. major* promastigotes (Lm-LUC) was injected subcutaneously at the base of the tail. The injection area was monitored until appearance of the lesion (approximately 6 weeks after injection), after which treatments were initiated. Groups of mice were treated once every two days for three weeks, one group with a direct plasma treatment and another with a direct He treatment. The APGD-j was placed approximately 3 mm above the surface of

the lesion, with a duty cycle of 10% and a He flow rate of 6 slm for 10 minutes. The mice were anesthetized with isofluorene before and during treatments.

3.3.3 Lesion Measurements

Pictures of the lesions were obtained on a weekly basis. The area of the open wound was measured using Adobe® Photoshop® CS6 Extended. First, the measurement scale was set in order to convert the pixel length to the length in centimeters, using a photographed ruler as a reference. Then, using the selection tools, the pixels corresponding to lesion area were selected, and the lesion area was recorded in centimeters squared (cm^2).

3.3.4 Measurement of parasite load

At the experimental endpoint of the study, the animals were euthanized using carbon dioxide (CO_2) and the skin lesions were collected to determine the parasitic load. The collected lesions were homogenized and the cells lysed using Firefly lysis buffer (Biotium). The luciferase assay was completed as described in section 3.2.8 above.

Chapter 4 : Results

4.1 Device characterization

4.1.1 OES

The emission spectrum of the APGD-j acquired at 5% duty cycle and 2 slm is shown in Figure 4.1 below.

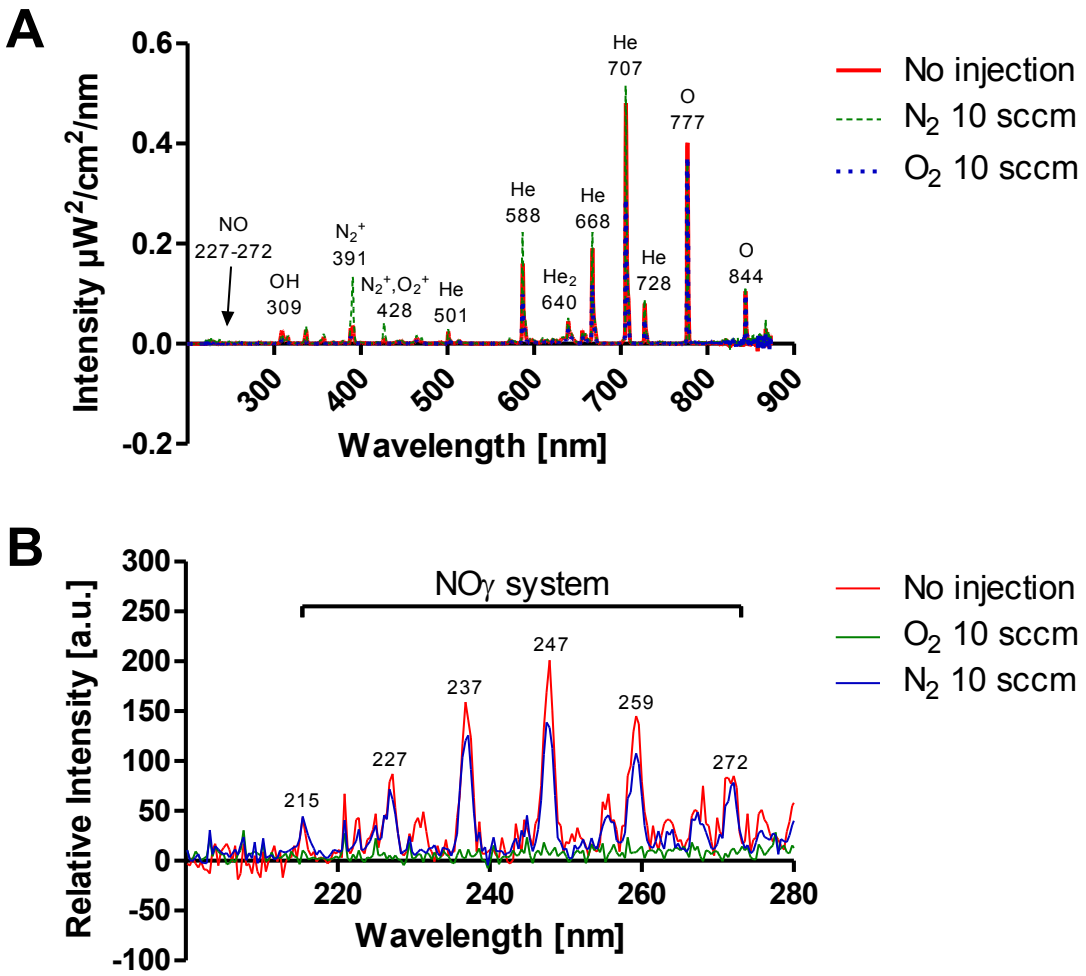

Figure 4.1: Emission spectrum of the APGD-j. A) The absolute intensity UV-VIS emission spectrum. B) The relative intensity UV emission spectrum. Source and wavelength of spectral lines are indicated.

Spectral lines and bands from a number of excited species can be observed. These include reactive oxygen and nitrogen species produced by the plasma, including atomic

oxygen, OH, and NO. All NO bands belong to the same band system, the NOγ (Nitrogen Third Positive) system (Figure 4.1B).

4.1.2 Nitrite concentration

Nitrite is one of two primary degradation products of NO in solution, and thus is representative of NO transfer from the APGD-j to *in vitro* culture media. The nitrite concentration of phenol red-free RPMI following APGD-j treatment was determined for various treatment times (**Erreur ! Source du renvoi introuvable.**). The experimental *in vitro* environments used in this study were mimicked using either 1 mL RPMI in a standard 12 well plate or 400 µL RPMI in a standard 24 well plate. The concentration of nitrite increased linearly with time for treatment times of up to 10 minutes.

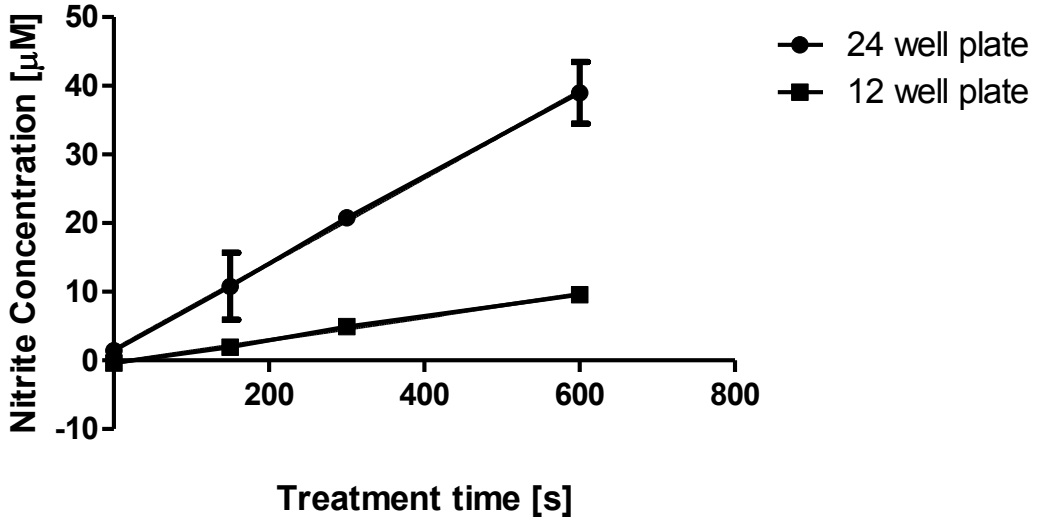

Figure 4.2: Nitrite concentration in RPMI following APGD-j treatment. Experiment performed in triplicate. Error bars represent standard deviation. 24-well plate: R2=0.96, P value<0.0001. 12-well plate: R2=0.98, P value<0.0001.

4.2 Effect of *in vitro* plasma treatments on B10R macrophages

4.2.1 Cell signalling

The first step of the investigation was to determine the short term effects of APGD-j treatments on cell signalling. Western blotting was used to determine the effect of the plasma treatment of the MAPK family. Macrophages were treated for 1, 5 and 10 min using direct and indirect treatments and incubated for 30 min (Figure 4.3 A & B).

Macrophages were also incubated for 15, 30, 60 and 120 min following 10 min direct or indirect treatments (Figure 4.3 C & D). All plasma treatments induced the phosphorylation of p38, and direct 10 minute plasma treatments induced the phosphorylation of JNK. Phosphorylation persisted for up to two hours after treatment. The results suggest ERK dephosphorylates from its basal level for all treatments including the He controls.

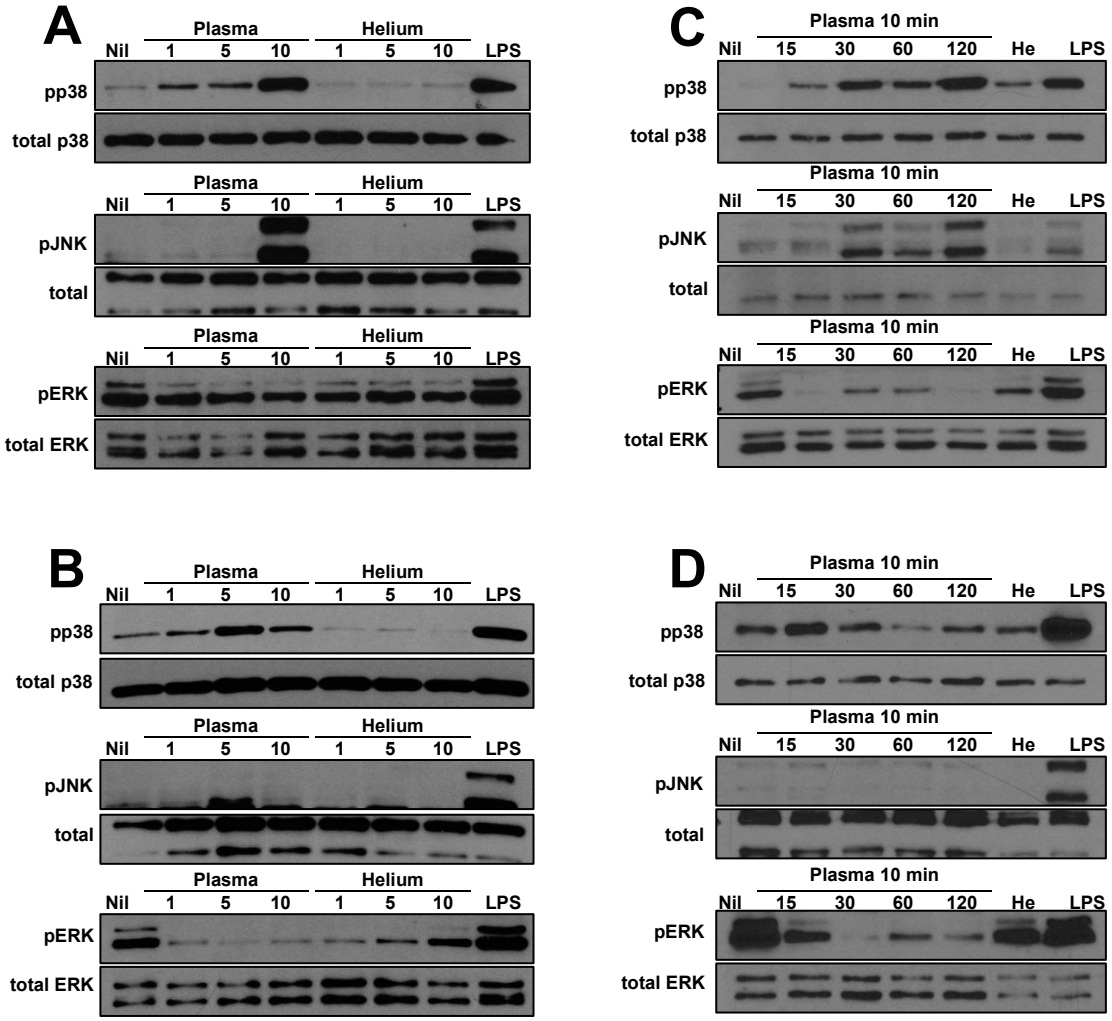

Figure 4.3: Direct and indirect plasma treatments of macrophages induce modulation of MAPK signalling. (A) Direct treatment at various treatment times (B) Indirect treatment at various incubation times (C) Time course following 10 minute direct treatment (D) Time course following 10 minute indirect treatment

4.2.2 Transcription factor translocation

Downstream of MAPK signalling proteins are transcription factors NF-κB and AP-1 which affect transcription of genes responsible for the immune response. The EMSA was used to determine if these transcription factors translocate into the nucleus following APGD-j treatment. Macrophages were treated indirectly for 10 minutes and incubated for 15, 30, 60 and 120 minutes. Although no change in NF-κB levels were observed (data not shown), AP-1 translocation did occur following treatment (Figure 4.4).

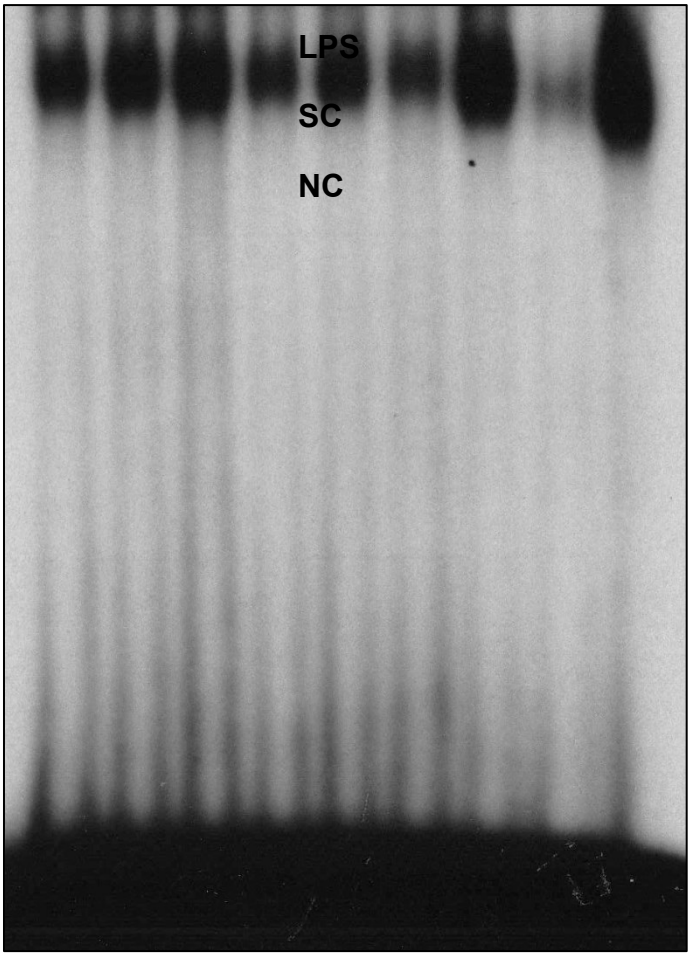

Figure 4.4: Transcription factor AP-1 inside the nucleus after indirect plasma treatment

4.2.3 Regulation of gene expression

Transcription factor translocation suggests modulation of gene expression as a consequence of APGD-j treatment. Thus, gene expression was investigated using qRT-PCR. 89 genes were studied with the RT^2 Profiler PCR Array System for mouse innate and adaptive immune responses. After a 10 minute indirect treatment, macrophages were incubated for 8 hours before RNA extraction. The fold up or down-regulation between the treated cells (Plasma, He as negative control and LPS as positive control) and the untreated cells for all tested genes is given in Table 4.1. In total, 25.8% of the genes assessed were modulated; 10 genes were up-regulated and 13 genes were downregulated by a factor of 2 or higher. Most notable were the upregulation of IL-1β, IL-1r1 and Nod1 by a factor of 27, 5.5 and 6 respectively. All the genes up or down-regulated by the APGD-j treatment are sorted by function in Table 4.2.

Table 4.1: The indirect plasma treatment modulates the expression of genes involved in the immune response of macrophages. This includes up-regulation of cytokine expression (IL1b, Il10, Csf2), modulation of pattern recognition receptors (The Tlr family, Nod1, Ddx58) Fold up or down regulation for each gene represents 3 biological replicates.

	Symbol	Plasma	He	LPS	Complete name
1	Apcs				Serum amyloid P-component
2	C3	-1.8	-1.1	1.9	Complement component 3
3	C5ar1	-1.9	1.1	**2.6**	Complement component 5a receptor 1
4	Casp1	1.4	1.1	1.8	Caspase 1
5	Ccl12	-1.5	-1.6	**17.7**	Chemokine (C-C motif) ligand 12
6	Ccl5	-1.5	-1.2	**124.1**	Chemokine (C-C motif) ligand 5
7	Ccr4	1.3	1.1	1.1	Chemokine (C-C motif) receptor 4
8	Ccr5	**-2.7**	-1.2	1.1	Chemokine (C-C motif) receptor 5
9	Ccr6	1.2	1.1	-1.0	Chemokine (C-C motif) receptor 6
10	Ccr8				Chemokine (C-C motif) receptor 8
11	Cd14	**3.1**	1.7	1.8	CD14 antigen
12	Cd4	1.1	1.2	-1.1	CD4 antigen
13	Cd40	**-3.7**	-1.3	**10.6**	CD40 antigen
14	Cd40lg	1.6	1.2	1.1	CD40 ligand
15	Cd80	**-2.6**	**-2.2**	1.6	CD80 antigen
16	Cd86	**-2.7**	-1.3	1.0	CD86 antigen
17	Cd8a	1.2	1.1	-1.0	CD8 antigen, alpha chain

18	Crp	1.1	1.1	-1.0	C-reactive protein, pentraxin-related
19	Csf2	**2.1**	1.8	1.3	Colony stimulating factor 2 (granulocyte-macrophage)
20	Cxcl10	-1.6	-1.2	**206.7**	Chemokine (C-X-C motif) ligand 10
21	Cxcr3	**-3.5**	-1.3	**-2.7**	Chemokine (C-X-C motif) receptor 3
22	Ddx58	**-3.8**	-1.7	**6.7**	DEAD (Asp-Glu-Ala-Asp) box polypeptide 58
23	Fasl	1.4	1.1	-1.1	Fas ligand (TNF superfamily, member 6)
24	Foxp3	1.2	1.3	-1.2	Forkhead box P3
25	Gata3	1.8	1.2	-1.1	GATA binding protein 3
26	H2-Q10	1.2	1.1	-1.0	Histocompatibility 2, Q region locus 10
27	H2-T23	2.0	-1.0	**7.3**	Histocompatibility 2, T region locus 23
28	Icam1	-1.0	1.1	**2.9**	Intercellular adhesion molecule 1
29	Ifna2	1.3	1.1	-1.1	Interferon alpha 2
30	Ifnar1	-1.5	-1.1	1.2	Interferon (alpha and beta) receptor 1
31	Ifnb1	-1.1	1.0	**10.7**	Interferon beta 1, fibroblast
32	Ifng				Interferon gamma
33	Ifngr1	-1.9	-1.1	-1.9	Interferon gamma receptor 1
34	Il10	**2.7**	1.1	**6.1**	Interleukin 10
35	Il13	1.3	1.1	-1.1	Interleukin 13
36	Il17a	1.2	1.1	-1.0	Interleukin 17A
37	Il18	**-2.6**	-1.5	**2.8**	Interleukin 18
38	Il1a	-1.2	-1.2	**2791.6**	Interleukin 1 alpha
39	Il1b	**27.1**	1.2	**2233.1**	Interleukin 1 beta
40	Il1r1	**5.5**	1.5	-1.2	Interleukin 1 receptor, type I
41	Il2	1.2	1.1	-1.0	Interleukin 2
42	Il23a	-1.1	1.0	**3.9**	Interleukin 23, alpha subunit p19
43	Il4	**2.4**	1.5	-1.3	Interleukin 4
44	Il5	1.2	1.1	-1.0	Interleukin 5
45	Il6	1.4	1.1	**702.3**	Interleukin 6
46	Irak1	-1.2	-1.0	-1.4	Interleukin-1 receptor-associated kinase 1
47	Irf3	1.3	1.1	-1.2	Interferon regulatory factor 3
48	Irf7	**-5.3**	-1.8	**21.1**	Interferon regulatory factor 7
49	Itgam	-1.6	1.1	-1.0	Integrin alpha M
50	Jak2	-1.3	-1.2	**3.8**	Janus kinase 2
51	Ly96	1.5	1.1	1.1	Lymphocyte antigen 96
52	Lyz2	1.4	1.3	-1.9	Lysozyme 2
53	Mapk1	1.4	1.2	-1.1	Mitogen-activated protein kinase 1
54	Mapk8	1.3	1.2	-1.0	Mitogen-activated protein kinase 8
55	Mbl2	1.2	1.1	-1.1	Mannose-binding lectin (protein C) 2
56	Mpo	1.2	1.1	-1.1	Myeloperoxidase
57	Mx1	-1.6	-1.7	**136.3**	Myxovirus (influenza virus) resistance 1
58	Myd88	1.5	1.0	1.4	Myeloid differentiation primary response gene 88

59	Nfkb1	-1.2	1.1	**2.4**	Nuclear factor of kappa light polypeptide gene enhancer in B-cells 1, p105
60	Nfkbia	1.9	1.3	**4.1**	Nuclear factor of kappa light polypeptide gene enhancer in B-cells inhibitor, alpha
61	Nlrp3	1.2	1.9	**7.1**	NLR family, pyrin domain containing 3
62	Nod1	**6.2**	1.6	**3.0**	Nucleotide-binding oligomerization domain containing 1
63	Nod2	-1.1	1.1	**7.0**	Nucleotide-binding oligomerization domain containing 2
64	Rag1		1.0	-1.0	Recombination activating gene 1
65	Rorc	1.3	-1.0	-1.3	RAR-related orphan receptor gamma
66	Slc11a1	-1.2	1.1	-1.0	Solute carrier family 11 (proton-coupled divalent metal ion transporters), member 1
67	Stat1	**-2.0**	-1.3	**3.5**	Signal transducer and activator of transcription 1
68	Stat3	1.7	1.3	1.8	Signal transducer and activator of transcription 3
69	Stat4	1.2	1.1	-1.1	Signal transducer and activator of transcription 4
70	Stat6	**-2.6**	-1.8	**-2.7**	Signal transducer and activator of transcription 6
71	Tbx21				T-box 21
72	Ticam1	1.3	1.3	1.4	Toll-like receptor adaptor molecule 1
73	Tlr1	**-2.0**	1.0	1.0	Toll-like receptor 1
74	Tlr2	-1.4	1.1	**3.1**	Toll-like receptor 2
75	Tlr3	**-2.1**	-1.2	**3.6**	Toll-like receptor 3
76	Tlr4	**2.0**	1.4	1.5	Toll-like receptor 4
77	Tlr5	-1.5	-1.1	**-2.7**	Toll-like receptor 5
78	Tlr6	1.2	-1.0	1.4	Toll-like receptor 6
79	Tlr7	**2.5**	1.7	1.5	Toll-like receptor 7
80	Tlr8	**2.9**	1.5	-1.5	Toll-like receptor 8
81	Tlr9	**-2.2**	-1.1	1.4	Toll-like receptor 9
82	Tnf	1.1	1.3	**5.8**	Tumor necrosis factor
83	Traf6	1.3	1.1	-1.1	Tnf receptor-associated factor 6
84	Tyk2	-1.6	-1.0	1.9	Tyrosine kinase 2
85	Actb	-1.1	-1.0	-1.0	Actin, beta
86	B2m	-1.2	-1.0	1.8	Beta-2 microglobulin
87	Gapdh	1.2	1.0	-1.1	Glyceraldehyde-3-phosphate dehydrogenase
88	Gusb	-1.1	-1.0	-1.4	Glucuronidase, beta
89	Hsp90ab1	1.2	1.0	-1.1	Heat shock protein 90 alpha (cytosolic), class B member 1

Table 4.2: Genes affected by the indirect plasma treatment sorted by function.

Groups of affected genes	Up-regulated	Down-regulated
Innate Immunity		
Pattern recognition receptors	**Nod1**, Tlr4, Tlr4, Tlr8	**Ddx58, Tlr1, Tlr9**, Tlr6
Cytokines	**Il1B**, Csf2	Il18
Other Genes	**H2-T23**, **Il1r1**, cd14	**C5ar1, Cd40, Irf7**, Stat1

Adaptive Immunity		
Th1 markers/Immune response	Tlr4	**Ccr5, Cxcr3**, Cd80, Il18, Tlr6
Th2 markers/ Immune response	**Il10**	Cd86, Il18, Stat6
Treg markers	**Il10**	
T cell activation		**Cd86**, Cd80
Cytokines	**Il10**	Il18
Other genes	**Il1B**, **Il1r1**	**Cd40, Irf7**, Stat1

4.3 Effect of *in vitro* plasma treatments on L. major

To assess the toxicity of the plasma treatments towards *L.* major, the cell wall integrity and cell metabolic activity of promastigotes following 5 minute direct and indirect APGD-j treatments were measured after an overnight incubation of the parasites. Cell wall integrity was determined by flow cytometry using PI staining (Figure 4.5A and B), and metabolic activity was measured using the XTT assay (Figure 4.5C). Ability of the surviving parasites to infect B10R macrophages and to survive the host immune response was determined following 6 hours of contact with the parasite suspension and 18 hours after rinsing the cells to remove un-internalised promastigotes (24 hours after the initial infection). The effects of direct and indirect plasma treatments were comparable. They both resulted in cell membrane disruption in approximately 50% of the treated population. Metabolic activity was similarly affected, with approximately 60% reduction in plasma treated parasites. However, both direct and indirect He controls resulted in a reduction of metabolic activity.

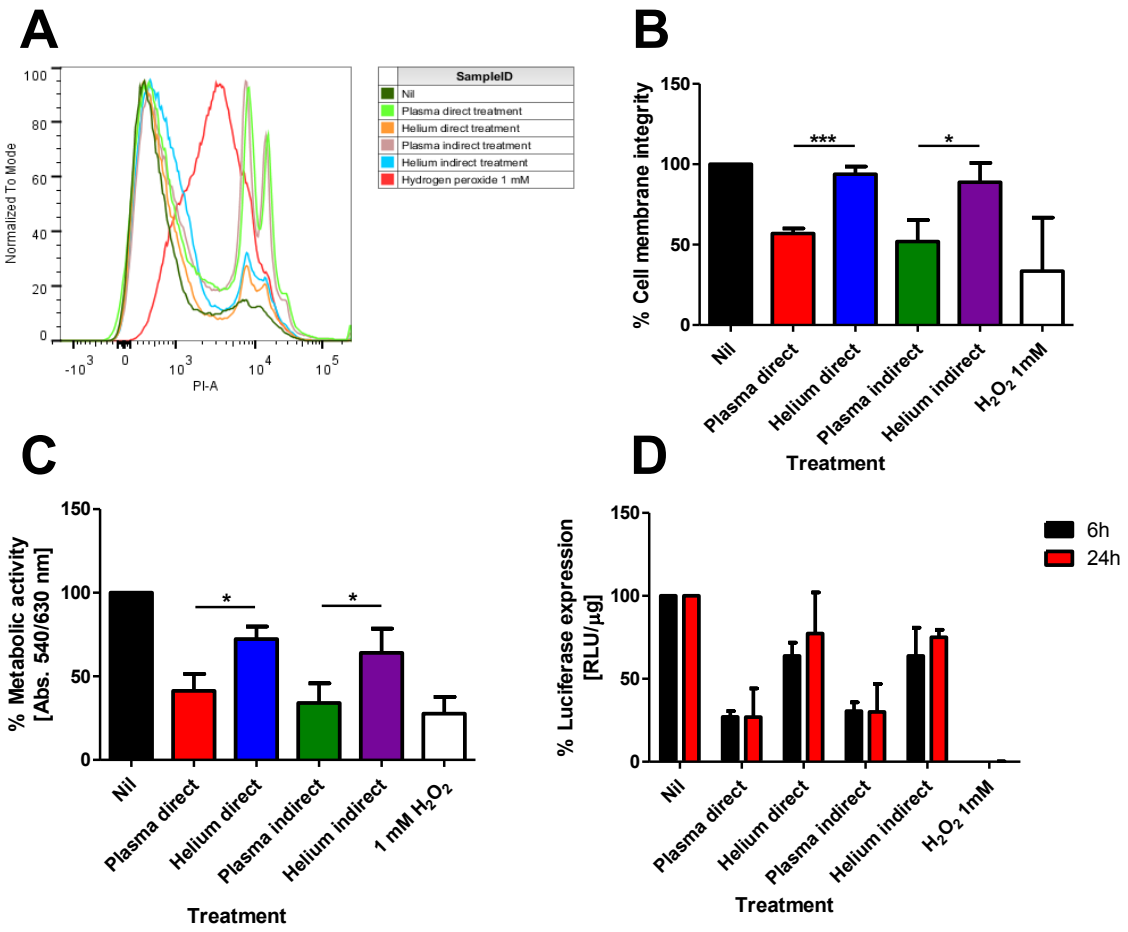

Figure 4.5: Viability of L. major following APGD-j treatment. (A) Representative experiment out of three biological replicates showing PI incorporation in treated cell populations. (B) Percentage of conserved cell membrane integrity as compared to the untreated sample. (C) Percentage of conserved metabolic activity as compared to the untreated sample. (D) Luciferase expression by internalized parasites 6 hours and 24 hours after the initial infection. Each column graph represents N=3 biological replicates with experiment done in duplicated. Plasma treatments and their respective He controls were compared using the unpaired t-test. *, **, *** represent $p<0.05$, 0.01, 0.001 respectively.

4.4 Plasma treatment of CL

The in vitro work was supplemented with an in vivo investigation on the effectiveness of plasma treatments on the growth of CL lesions in BALB/c mice infected with L. major. Treatments began immediately after the appearance of the papule. The area of the open wound was recorded weekly (Figure 4.6A, B and Figure 4.7) and the parasite load was assessed at the experimental endpoint (Figure 4.6C). The lesion sizes on week 5 were significantly smaller for the plasma treated group than for the helium control group, but the plasma treatments had no effect on parasite load. This suggests that the plasma had an effect on the pathogenesis of the disease, but no effect on the infection.

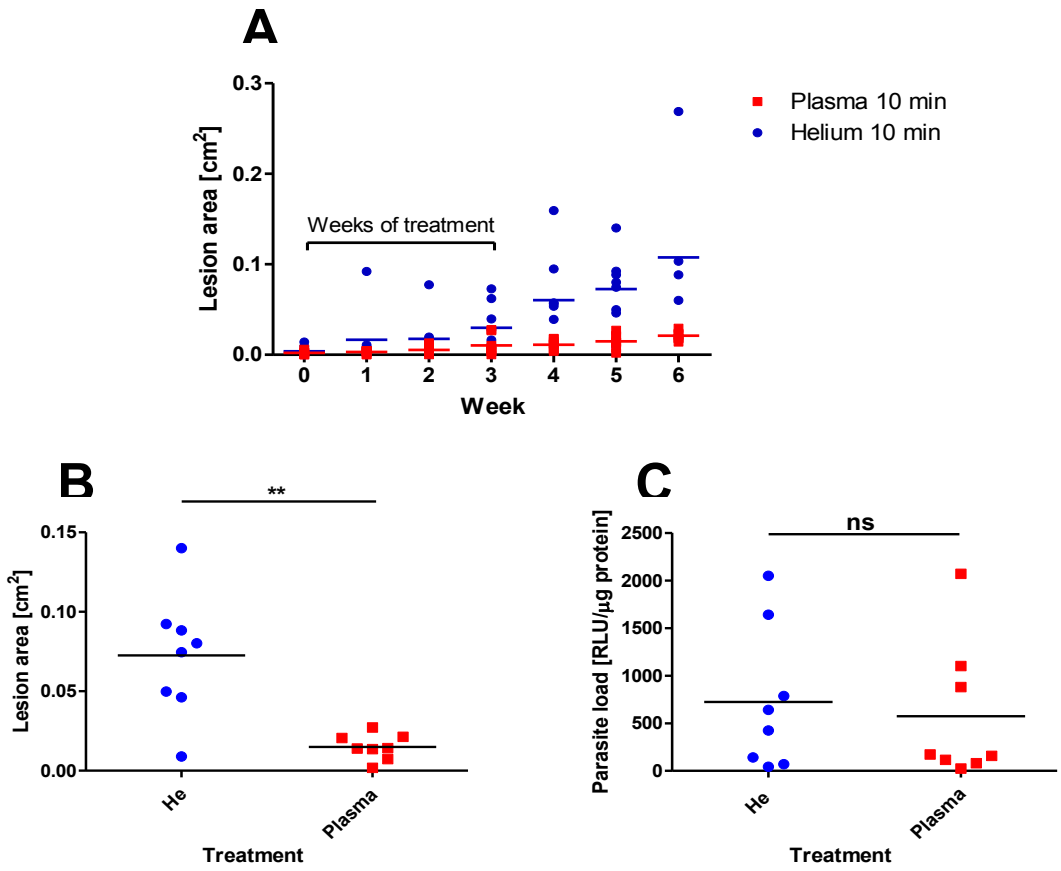

Figure 4.6: Plasma treatments decelerate CL lesion growth without affecting parasite load in BALB/c mice infected with *L. major* (A) Weekly progression of lesion size. N=8 biological replicates up to week 5, with n=5 and n=6 for the helium and plasma groups on week 6, respectively. (B) The lesion areas on week 5 and (C) the parasite load at the experimental endpoint. ns, *, **, *** represent $p>0.05$, $p<0.05$, $p<0.01$, $p<0.001$ respectively,

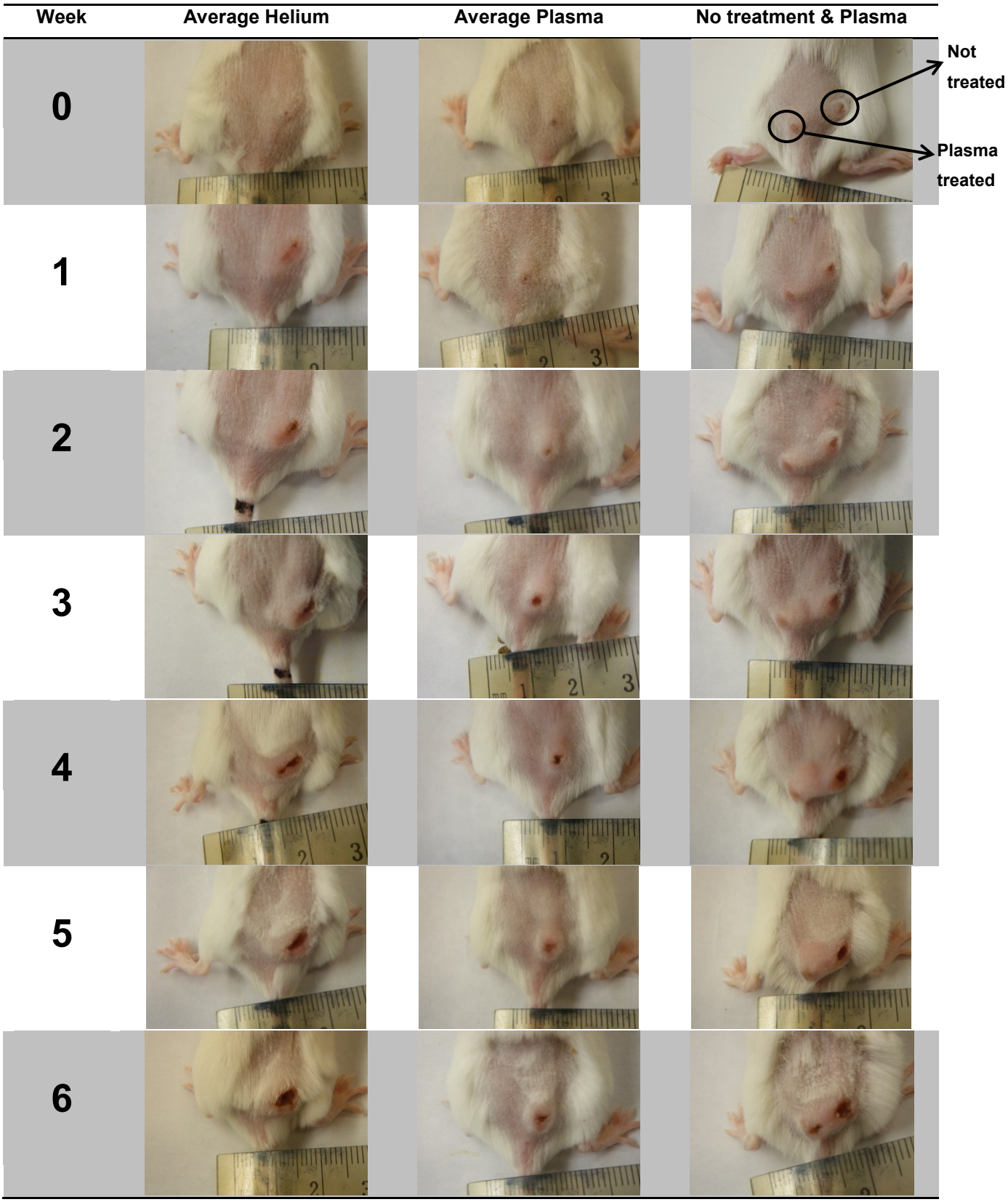

Figure 4.7: The evolution of the average-sized helium and plasma lesions.

Chapter 5 : Discussion

The aim of this investigation was to develop a ROS and NO producing plasma device and explore its potential as a treatment for CL. Given the lack of previous research on the subject, the results presented herein should be considered preliminary. Both *in vitro* and *in vivo* experimental models were employed. The murine macrophage cell line B10R was chosen given that the primary cellular hosts of *Leishmania* parasites during infection are macrophages, and B10R cells have been used extensively in leishmaniasis research[76-78]. Treatments of B10Rs *in vitro* were used to determine whether NAPP could activate macrophages. A special focus was given to signalling pathways which are downregulated by *Leishmania* species. The Lm-LUC line of *Leishmania* promastigotes (*L. major* strain stably transfected with the luciferase reporter gene) was chosen to enable the use luciferase assays to evaluate parasitic load. Two types of *in vitro* treatments were employed: direct treatments of the media containing the cells, and indirect treatments where the media was treated immediately before it was used in cell culture. This effectively isolated the effects of the reactive species transferred into the extracellular environment from the other plasma-related effects (UV radiation, shear stress, etc.). The mouse model chosen for this investigation was the infection of BALB/c mice with Lm-LUC parasites at the base of the tail. Promastigotes were administered via cutaneous injection. This model was chosen to replicate progressive, non-curing clinical manifestations of CL[79].

It was demonstrated using optical emission spectroscopy that the device developed for this experiment, the APGD-j, successfully produces atomic oxygen, OH and NO. The APGD-j was designed to allow the injection of gases into the plasma forming region, and both nitrogen and oxygen injections were assessed. Figure 4.1 shows the emission spectra in the UV and visible ranges with no gas injection, 10 sccm nitrogen injection and 10 sccm oxygen injection through the capillary. The production of nitrogen and oxygen species without capillary gas injection suggests significant air entrainment into the nozzle of the device, and the presence of OH is due to air moisture. As a rule, the intensity of the spectrum decreases when injecting reactive gases through the capillary. Therefore, oxygen and nitrogen injection were not used for subsequent experiments. It is worth

noting however that the choice of injected gas has an important effect on the relative emission of the various bands, as seen in Figure 4.1A. Experimenting with nozzle design and reactive gas injection in a controlled environment would be required for full device optimization. All the NO bands belong to the same band system, the NOγ (Nitrogen Third Positive) system. This is in accordance with the results presented by Boudam *et al*, who state that NOβ emission does not occur at atmospheric pressure due to an alternate de-excitation path, collisional quenching with N_2, which is more efficient at higher pressures.

The nitrite concentration was determined in RPMI following APGD-j treatment in order to perform a preliminary assessment of reactive species transfer into the extracellular environment during *in vitro* experiments. Both *in vitro* experimental conditions used in this investigation were tested, namely 1 mL of RPMI in a 12-well plate and 400 µL of RPMI in a 24-well plate (**Erreur ! Source du renvoi introuvable.**). In both cases, treatment of the liquid resulted in an increase in nitrite proportional to treatment time. The effect of liquid evaporation was evaluated using a He only control, which showed no increase in nitrite concentration compared to untreated RPMI.

The effects of APGD-j treatments on B10R macrophages were studied using a sequential, upstream-to-downstream strategy, by assessing signalling proteins, transcription factors and finally gene expression. The pathways of interest were those affected by *Leishmania* infection. First, the effect of plasma treatments on the MAPK family of signalling proteins was assessed using Western Blotting (Figure 4.3). For direct treatments, both p38 and JNK were phosphorylated following treatment, with p38 after as little as a 1 minute treatment, and JNK after a 10 minute treatment. Both signals persisted for up to 2 hours after treatment. p38 phosphorylation also occurred following indirect treatments, suggesting that this pathway is activated by reactive species transferred to the media. In contrast, indirect treatments failed to phosphorylate JNK. Given that direct He treatments also did not activate this pathway, it is probable that UV radiation is responsible for JNK phosphorylation. These two conclusions are supported by literature, given that intracellular ROS have been found to induce phosphorylation of p38 in macrophages[80] and other cell types[81], and UV radiation is a well-known strong activator of the JNK

pathway[82-84]. The effects of the treatments on ERK are difficult to interpret, since all treatments, including direct and indirect He treatments, result in a dephorphorylation of ERK from its basal levels. The degree of dephosphorylation was inconsistent, and basal levels of ERK were unusually high. A hypothetical reason for this result is that a component of RPMI in solution which induced the phosphorylation of ERK is affected when shear stress is applied to the liquid. As with p38, intracellular ROS has also shown to activate ERK in macrophages[80]. Additionally, NAPP treatments were shown to induce the phosphorylation of all three of these MAPK in both $CD4^{+}$T helper cell and monocyte cell lines[85]. The discrepancies in the results could potentially be attributed to the type and concentration of ROS as well as the choice of cell line. There are several proposed hypotheses for MAPK activation by ROS, including activation of upstream signalling proteins (e.g. redox sensitive MAP3Ks and MAPK2Ks) or the inhibition of MAPK photphatases, including PTPs[86]. Studies have shown that *Leishmania* promastigote and amastigotes do not activate the MAPK signalling pathways[71], and can prevent the activation of p38[87], ERK[88] and JNK[71] in activated cells. Several mechanisms of MAPK signalling downregulation by *Leishmania* have been put forth. One study demonstrated the degradation of ERK and JNK in macrophages following L. Mexicana infection, with p38 remaining intact yet still inactivated by infection[89]. Another demonstrated that infection by LPG deficient *L. donovani* promastigotes eliminated the inhibition of ERK activation[71]. The most likely cause of MAPK signal impairment is the activation of protein tyrosine phosphatases (PTPs) by the parasite, as demonstrated by numerous studies[88, 90]. Therefore, plasma induced redox signalling could potentially counter the inhibitory effect of *Leishmania* species on MAPK. In order to confirm signal transduction downstream of the modulated MAPK, the translocation of transcription factors NF-κB and AP-1 were assessed using the EMSA following an indirect 10 minute treatment. No translocation of NF-κB was observed, however a transient increase of AP-1 was found inside the nucleus (Figure 4.4). This result was expected, given that p38 and JNK are generally responsible for inducing AP-1 following stress-related stimuli[91].

Given evidence of signalling cascade activation and transcription factor translocation, gene expression modulation following APGD-j treatment was assessed using qRT-PCR.

RT^2 Profiler PCR Array System for mouse innate and adaptive immune responses was chosen in order to assess the effect of the treatment on genes relevant to macrophage activation. Out of the 89 genes tested (Table 1.1), 10 (11.2%) were upregulated and 13 (14.6%) were downregulated by a factor of 2 or more, compared to 27 (30.3%) and 3 (3.4%) for LPS. The most significant fold change was that of Interleukin-1 beta (IL-1β), a pro-inflammatory cytokine, which was upregulated 27 fold following treatment. Studies have previously linked the p38 signalling cascade with IL-1β gene expression[92]. Interleukin-receptor, type 1 (IL-1r1), the receptor for IL-1β, was also increased following treatment. Another up-regulated cytokine was Interleukin-10 (IL-10) Although production of IL-10 has previously been associated with the inability to control CL infection, one study demonstrated that it is IL-10 production by Th1 cells, not by macrophages, which cause immune suppression[93]. Globally, it is difficult to distinguish a distinct pattern of macrophage function modulation after plasma treatment, but given the high up-regulation of IL-1β, the effect of plasma treatments on macrophages is probably pro-inflammatory. A more reliable statement would be that plasma treatments lead to changes in immune system gene expression in B10R macrophages.

The antileishmanial activity of NO and ROS has been extensively reported, as reviewed by Van Assche *et al.*[94]. Superoxide, NO, hydrogen peroxide and peroxinitrite have all demonstrated *Leishmania* promastigote killing *in vitro*. Killing of promastigotes by APGD-j treatment was therefore expected. Following treatment, cell wall integrity was assessed by flow cytometry (Figure 4.5A and B) and metabolic activity using the XTT assay (Figure 4.5C). There was no discernible difference between the effects of the direct and indirect treatments, suggesting that the mechanism of parasite killing was modulated by one or several of the reactive species transferred into the media. The luciferase assay (Figure 4.5D) demonstrates that the surviving parasites remained infectious, with neither parasite internalization or parasite clearance by the macrophage being affected, in contrast with the hydrogen peroxide treated control where no infection was established following treatment.

The purpose of the *in vivo* investigation was to evaluate the effect of APGD-j treatments on both lesion progression and parasite burden, with the hope that the plasma would have

a therapeutic effect on the lesion pathology and on the extent of infection. The results demonstrate that APGD-j treatments significantly reduced the spread of ulceration of the wound by the 5^{th} week (Figure 4.6B). However, they had no significant effect on parasite load (Figure 4.6C). Cases of high parasite load without ulcerations have been reported in literature. Examples include HIV/*Leishmania* co-infections[95] and the clinical manifestation named diffuse leishmaniasis[68]. Of particular interest is the study by Giannini on the effects of UV-B radiation on CL infections by *L. major*[96]. Lesions were treated with a dose of 15 mJ/cm^2 at 24 hours before infection and every 48 to 72 hours following infection for one month, resulting in significant suppression of lesion growth compared to the control group. Terabe *et al.* demonstrated that ulceration of CL nodules did not occur without $CD4^+$ expression in immunodeficient mice after inoculation with *L. amazonensis* which was independent of parasite load[97]. Their study infers that $CD4^+$ T cells are responsible for the pathogenesis of the disease, which explains the absence of ulceration for HIV/*Leishmania* co-infections (HIV infections result in low levels of $CD4^+$). A possible reason for the slower ulceration of the treated lesions is therefore a change in T cell recruitment or differentiation, but the exact mechanisms behind the effects described here cannot be fully understood without further experimentation. Nevertheless, given that large ulcers and the subsequent scarring are the source of disfigurement and psychological damage which accompany CL infections, APGD-j treatments, once optimized, could prove extremely beneficial in the management of the disease.

Chapter 6 : Conclusions and Future Perspectives

This work was a preliminary study of the use of a non-thermal atmospheric pressure plasma jet as a treatment for cutaneous leishmaniasis. To this end, the *in vitro* interactions of the APGD-j with B10R macrophages and with luciferase expressing *Leishmania major* promastigotes were investigated, and the effectiveness of APGD-j treatments on CL wounds *in vivo* was studied using the BALB/c mouse model. It was demonstrated that both direct and indirect treatments induce the phosphorylation of p38, and direct treatments induce the phosphorylation of JNK. An increase in the translocation of transcription factor AP-1 to the nucleus was also observed following indirect treatments, confirming the activation of a stress induced MAPK signalling cascade. A study of immunity related gene expression following indirect plasma treatments demonstrated the modulation of 23 genes, including the strong up-regulation of IL-1β, a pro-inflammatory cytokine. APGD-j treatments resulted in a significant decrease of the viable population in a suspension of *L. major* promastigotes, which was attributed to the reactive species transferred into the media. The *in vivo* experiment demonstrated that the APGD-j treatment of CL lesions resulted in a significant reduction in ulceration; however, this result was not accompanied by a reduction in parasite load. Ulcer size management is still a promising result, and further investigations into the potential of APGD-j treatments to manage CL infections are warranted. The topics of such investigations could include: (1) a further characterization and optimization of the APGD-j, (2) a further characterization and optimization of plasma treated media with respect to ROS and NO concentrations following treatment, (3) the mechanisms of MAPK cascade activation by plasma treatments, (4) the production of cytokines and chemokines by B10Rs following plasma treatment, (5) the effects of the plasma treatments on other macrophage functions including proliferation/apoptosis and (6) the effects of plasma treatments on macrophages infected with leishmaniasis. Although there is still much research to be done before the potential of plasma treatments can be properly assessed, hopefully these preliminary results give insight into a previously untapped application of non-thermal plasmas.

References

1. Kong, M.G., et al., *Plasma medicine: an introductory review.* New Journal of Physics, 2009. **11**: p. 115012.
2. Bruch-Gerharz, D., T. Ruzicka, and V. Kolb-Bachofen, *Nitric oxide in human skin: current status and future prospects.* Journal of investigative dermatology, 1998. **110**(1): p. 1-7.
3. Graves, D.B., *The emerging role of reactive oxygen and nitrogen species in redox biology and some implications for plasma applications to medicine and biology.* Journal of Physics D: Applied Physics, 2012. **45**(26): p. 263001.
4. Fridman, G., et al., *Applied plasma medicine.* Plasma Processes and Polymers, 2008. **5**(6): p. 503-533.
5. Dobrynin, D., et al., *Direct and controllable nitric oxide delivery into biological media and living cells by a pin-to-hole spark discharge (PHD) plasma.* Journal of Physics D: Applied Physics, 2011. **44**: p. 075201.
6. Isbary, G., et al., *Successful and safe use of 2 min cold atmospheric argon plasma in chronic wounds: results of a randomized controlled trial.* British Journal of Dermatology, 2012.
7. Vandamme, M., et al., *Response of human glioma U87 xenografted on mice to non thermal plasma treatment.* Plasma Medicine, 2011. **1**(1): p. 27-43.
8. Keidar, M., et al., *Cold plasma selectivity and the possibility of a paradigm shift in cancer therapy.* British journal of cancer, 2011. **105**(9): p. 1295-1301.
9. Olivier, M., D.J. Gregory, and G. Forget, *Subversion mechanisms by which Leishmania parasites can escape the host immune response: a signaling point of view.* Clinical Microbiology Reviews, 2005. **18**(2): p. 293-305.
10. Kim, K.H. and R.G. Geronemus, *Nonablative laser and light therapies for skin rejuvenation.* Archives of Facial Plastic Surgery, 2004. **6**(6): p. 398.
11. Grimm, I.S., *Argon Plasma Coagulation.* Handbook of gastroenterologic procedures, 2005. **236**: p. 235.

12. Foest, R., M. Schmidt, and K. Becker, *Microplasmas, an emerging field of low-temperature plasma science and technology.* International Journal of Mass Spectrometry, 2006. **248**(3): p. 87-102.
13. Madou, M.J., *Manufacturing Techniques for Microfabrication and Nanotechnology*2012: CRC Press.
14. Napartovich, A., *Overview of atmospheric pressure discharges producing nonthermal plasma.* Plasmas and polymers, 2001. **6**(1): p. 1-14.
15. Stoffels, E., Y. Sakiyama, and D.B. Graves, *Cold atmospheric plasma: charged species and their interactions with cells and tissues.* Plasma Science, IEEE Transactions on, 2008. **36**(4): p. 1441-1457.
16. Walsh, J.L. and M.G. Kong, *Contrasting characteristics of linear-field and cross-field atmospheric plasma jets.* Applied Physics Letters, 2008. **93**(11): p. 111501-111501-3.
17. Zelle, M., *Biological effects of ultraviolet radiation.* Medical Electronics, IRE Transactions on, 1960(3): p. 130-135.
18. Edwards, R. and K.G. Harding, *Bacteria and wound healing.* Current opinion in infectious diseases, 2004. **17**(2): p. 91-96.
19. Nosenko, T., T. Shimizu, and G. Morfill, *Designing plasmas for chronic wound disinfection.* New Journal of Physics, 2009. **11**: p. 115013.
20. Laroussi, M., *Nonthermal decontamination of biological media by atmospheric-pressure plasmas: Review, analysis, and prospects.* Plasma Science, IEEE Transactions on, 2002. **30**(4): p. 1409-1415.
21. Laroussi, M. and F. Leipold, *Evaluation of the roles of reactive species, heat, and UV radiation in the inactivation of bacterial cells by air plasmas at atmospheric pressure.* International Journal of Mass Spectrometry, 2004. **233**(1-3): p. 81-86.
22. Choi, J.H., et al., *Analysis of sterilization effect by pulsed dielectric barrier discharge.* Journal of electrostatics, 2006. **64**(1): p. 17-22.
23. Birmingham, J.G., *Mechanisms of bacterial spore deactivation using ambient pressure nonthermal discharges.* Plasma Science, IEEE Transactions on, 2004. **32**(4): p. 1526-1531.

24. Lu, X.P., et al., *The roles of the various plasma agents in the inactivation of bacteria.* Journal of Applied Physics, 2008. **104**(5): p. 053309-053309-5.
25. Gweon, B., et al., *Escherichia coli deactivation study controlling the atmospheric pressure plasma discharge conditions.* Current Applied Physics, 2009. **9**(3): p. 625-628.
26. Deng, X., J. Shi, and M.G. Kong, *Physical mechanisms of inactivation of Bacillus subtilis spores using cold atmospheric plasmas.* Plasma Science, IEEE Transactions on, 2006. **34**(4): p. 1310-1316.
27. Boudam, M., et al., *Bacterial spore inactivation by atmospheric-pressure plasmas in the presence or absence of UV photons as obtained with the same gas mixture.* Journal of Physics D: Applied Physics, 2006. **39**: p. 3494.
28. Kalghatgi, S., et al., *Effects of non-thermal plasma on mammalian cells.* PLoS ONE, 2011. **6**(1): p. e16270.
29. Perni, S., et al., *Probing bactericidal mechanisms induced by cold atmospheric plasmas with Escherichia coli mutants.* Applied physics letters, 2007. **90**: p. 073902.
30. Leduc, M., et al., *Effects of Non-thermal Plasmas on DNA and Mammalian Cells.* Plasma Processes and Polymers, 2010. **7**(11): p. 899-909.
31. Yan, X., et al., *Plasma-Induced Death of HepG2 Cancer Cells: Intracellular Effects of Reactive Species.* Plasma Processes and Polymers, 2011.
32. Laroussi, M., D. Mendis, and M. Rosenberg, *Plasma interaction with microbes.* New Journal of Physics, 2003. **5**: p. 41.
33. Kieft, I. and E. Stoffels, *Electrical and optical characterization of the plasma needle.* New Journal of Physics, 2004. **6**: p. 149.
34. Stoffels, E., et al., *Plasma needle for in vivo medical treatment: recent developments and perspectives.* Plasma Sources Science and Technology, 2006. **15**: p. S169.
35. Sladek, R. and E. Stoffels, *Deactivation of Escherichia coli by the plasma needle.* Journal of Physics D: Applied Physics, 2005. **38**: p. 1716.

36. Goree, J., et al., *Killing of S. mutans bacteria using a plasma needle at atmospheric pressure.* Plasma Science, IEEE Transactions on, 2006. **34**(4): p. 1317-1324.
37. Sladek, R., et al., *Treatment of Streptococcus mutans biofilms with a nonthermal atmospheric plasma.* Letters in applied microbiology, 2007. **45**(3): p. 318-323.
38. Stoffels, E., I. Kieft, and R. Sladek, *Superficial treatment of mammalian cells using plasma needle.* Journal of Physics D: Applied Physics, 2003. **36**: p. 2908.
39. Kieft, I.E., M. Kurdi, and E. Stoffels, *Reattachment and apoptosis after plasma-needle treatment of cultured cells.* Plasma Science, IEEE Transactions on, 2006. **34**(4): p. 1331-1336.
40. Stoffels, E., A.J.M. Roks, and L.E. Deelman, *Delayed effects of cold atmospheric plasma on vascular cells.* Plasma Processes and Polymers, 2008. **5**(6): p. 599-605.
41. Fridman, G., et al., *Blood coagulation and living tissue sterilization by floating-electrode dielectric barrier discharge in air.* Plasma Chemistry and Plasma Processing, 2006. **26**(4): p. 425-442.
42. Fridman, G., et al., *Floating electrode dielectric barrier discharge plasma in air promoting apoptotic behavior in melanoma skin cancer cell lines.* Plasma Chemistry and Plasma Processing, 2007. **27**(2): p. 163-176.
43. Kalghatgi, S., et al., *Endothelial cell proliferation is enhanced by low dose non-thermal plasma through fibroblast growth factor-2 release.* Annals of biomedical engineering, 2010. **38**(3): p. 748-757.
44. Laroussi, M. and X. Lu, *Room-temperature atmospheric pressure plasma plume for biomedical applications.* Applied Physics Letters, 2005. **87**(11): p. 113902-113902-3.
45. Laroussi, M., et al., *Inactivation of bacteria by the plasma pencil.* Plasma processes and polymers, 2006. **3**(6-7): p. 470-473.
46. Karakas, E., et al., *Destruction of α-synuclein based amyloid fibrils by a low temperature plasma jet.* Applied Physics Letters, 2010. **97**: p. 143702.
47. Leveille, V. and S. Coulombe, *Design and preliminary characterization of a miniature pulsed RF APGD torch with downstream injection of the source of reactive species.* Plasma Sources Science and Technology, 2005. **14**: p. 467.

48. Léveillé, V. and S. Coulombe, *Atomic Oxygen Production and Exploration of Reaction Mechanisms in a He-O2 Atmospheric Pressure Glow Discharge Torch.* Plasma Processes and Polymers, 2006. **3**(8): p. 587-596.
49. Léveillé, V. and S. Coulombe, *Electrical probe calibration and power calculation for a miniature 13.56 MHz plasma source.* Measurement Science and Technology, 2006. **17**: p. 3027.
50. Yonson, S., et al., *Cell treatment and surface functionalization using a miniature atmospheric pressure glow discharge plasma torch.* Journal of Physics D: Applied Physics, 2006. **39**: p. 3508.
51. Leduc, M., et al., *Cell permeabilization using a non-thermal plasma.* New Journal of Physics, 2009. **11**: p. 115021.
52. Pacher, P., J.S. Beckman, and L. Liaudet, *Nitric oxide and peroxynitrite in health and disease.* Physiological reviews, 2007. **87**(1): p. 315-424.
53. Beckman, J.S. and W.H. Koppenol, *Nitric oxide, superoxide, and peroxynitrite: the good, the bad, and ugly.* American Journal of Physiology-cell physiology, 1996. **271**(5): p. C1424-C1437.
54. Bedard, K. and K.-H. Krause, *The NOX family of ROS-generating NADPH oxidases: physiology and pathophysiology.* Physiological reviews, 2007. **87**(1): p. 245-313.
55. Lambeth, J.D., *NOX enzymes and the biology of reactive oxygen.* Nature Reviews Immunology, 2004. **4**(3): p. 181-189.
56. Klebanoff, S.J., *Myeloperoxidase: friend and foe.* Journal of leukocyte biology, 2005. **77**(5): p. 598-625.
57. Winterbourn, C.C., *Reconciling the chemistry and biology of reactive oxygen species.* Nature chemical biology, 2008. **4**(5): p. 278-286.
58. Bogdan, C., *Nitric oxide and the immune response.* Nature immunology, 2001. **2**(10): p. 907-916.
59. Bogdan, C., M. Röllinghoff, and A. Diefenbach, *Reactive oxygen and reactive nitrogen intermediates in innate and specific immunity.* Current opinion in immunology, 2000. **12**(1): p. 64-76.

60. Jay Forman, H. and M. Torres, *Redox signaling in macrophages.* Molecular aspects of medicine, 2001. **22**(4): p. 189-216.
61. Witte, M.B. and A. Barbul, *Role of nitric oxide in wound repair.* The American Journal of Surgery, 2002. **183**(4): p. 406-412.
62. Organization, W.H., *Control of the leishmaniases: report of a meeting of the WHO Expert Committee on the Control of Leishmaniases*2010: World Health Organization.
63. Alvar, J., et al., *Leishmaniasis worldwide and global estimates of its incidence.* PLoS ONE, 2012. **7**(5): p. e35671.
64. Reithinger, R., et al., *Cutaneous leishmaniasis.* The Lancet infectious diseases, 2007. **7**(9): p. 581-596.
65. Kaye, P. and P. Scott, *Leishmaniasis: complexity at the host–pathogen interface.* Nature Reviews Microbiology, 2011. **9**(8): p. 604-615.
66. Kamhawi, S., *Phlebotomine sand flies and< i> Leishmania</i> parasites: friends or foes?* Trends in parasitology, 2006. **22**(9): p. 439-445.
67. Hepburn, N., *Cutaneous leishmaniasis.* Clinical and experimental dermatology, 2000. **25**(5): p. 363-370.
68. Dowlati, Y., *Cutaneous leishmaniasis: clinical aspect.* Clinics in dermatology, 1996. **14**(5): p. 425-431.
69. Antoine, J.-C., et al., *The biogenesis and properties of the parasitophorous vacuoles that harbour< i> Leishmania</i> in murine macrophages.* Trends in microbiology, 1998. **6**(10): p. 392-401.
70. Nandan, D. and N.E. Reiner, *Attenuation of gamma interferon-induced tyrosine phosphorylation in mononuclear phagocytes infected with Leishmania donovani: selective inhibition of signaling through Janus kinases and Stat1.* Infection and Immunity, 1995. **63**(11): p. 4495-4500.
71. Privé, C. and A. Descoteaux, *Leishmania donovani promastigotes evade the activation of mitogen-activated protein kinases p38, c-Jun N-terminal kinase, and extracellular signal-regulated kinase-1/2 during infection of naive macrophages.* European journal of immunology, 2000. **30**(8): p. 2235-2244.

72. Gomez, M.A., et al., *Leishmania GP63 alters host signaling through cleavage-activated protein tyrosine phosphatases.* Science signaling, 2009. **2**(90): p. ra58.
73. Kholodenko, B.N., *Cell-signalling dynamics in time and space.* Nature reviews Molecular cell biology, 2006. **7**(3): p. 165-176.
74. Tripathi, P., V. Singh, and S. Naik, *Immune response to Leishmania: paradox rather than paradigm.* FEMS Immunology & Medical Microbiology, 2007. **51**(2): p. 229-242.
75. Roy, G., et al., *Episomal and stable expression of the luciferase reporter gene for quantifying< i> Leishmania</i> spp. infections in macrophages and in animal models.* Molecular and biochemical parasitology, 2000. **110**(2): p. 195-206.
76. Matte, C. and M. Olivier, *Leishmania-induced cellular recruitment during the early inflammatory response: modulation of proinflammatory mediators.* Journal of Infectious Diseases, 2002. **185**(5): p. 673-681.
77. Gregory, D.J., et al., *A novel form of NF-κB is induced by Leishmania infection: Involvement in macrophage gene expression.* European journal of immunology, 2008. **38**(4): p. 1071-1081.
78. Forget, G., et al., *Role of host protein tyrosine phosphatase SHP-1 in Leishmania donovani-induced inhibition of nitric oxide production.* Infection and immunity, 2006. **74**(11): p. 6272-6279.
79. Sacks, D.L. and P.C. Melby, *Animal models for the analysis of immune responses to leishmaniasis.* Current protocols in immunology, 2001: p. 19.2. 1-19.2. 20.
80. Ogura, M. and M. Kitamura, *Oxidant stress incites spreading of macrophages via extracellular signal-regulated kinases and p38 mitogen-activated protein kinase.* The Journal of Immunology, 1998. **161**(7): p. 3569-3574.
81. McCubrey, J.A., M.M. LaHair, and R.A. Franklin, *Reactive oxygen species-induced activation of the MAP kinase signaling pathways.* Antioxidants & redox signaling, 2006. **8**(9-10): p. 1775-1789.
82. Devary, Y., et al., *Rapid and preferential activation of the c-jun gene during the mammalian UV response.* Molecular and cellular biology, 1991. **11**(5): p. 2804-2811.

83. Hibi, M., et al., *Identification of an oncoprotein-and UV-responsive protein kinase that binds and potentiates the c-Jun activation domain.* Genes & Development, 1993. **7**(11): p. 2135-2148.

84. Dérijard, B., et al., *JNK1: a protein kinase stimulated by UV light and Ha-Ras that binds and phosphorylates the c-Jun activation domain.* Cell, 1994. **76**(6): p. 1025-1037.

85. Bundscherer, L., et al., *Impact of non-thermal plasma treatment on MAPK signaling pathways of human immune cell lines.* Immunobiology, 2013.

86. Son, Y., et al., *Mitogen-activated protein kinases and reactive oxygen species: how can ROS activate MAPK pathways?* Journal of signal transduction, 2011. **2011**.

87. Awasthi, A., et al., *CD40 Signaling Is Impaired in L. major–infected Macrophages and Is Rescued by a p38MAPK Activator Establishing a Host-protective Memory T Cell Response.* The Journal of experimental medicine, 2003. **197**(8): p. 1037-1043.

88. Nandan, D., R. Lo, and N.E. Reiner, *Activation of phosphotyrosine phosphatase activity attenuates mitogen-activated protein kinase signaling and inhibits c-FOS and nitric oxide synthase expression in macrophages infected with Leishmania donovani.* Infection and Immunity, 1999. **67**(8): p. 4055-4063.

89. Cameron, P., et al., *Inhibition of lipopolysaccharide-induced macrophage IL-12 production by Leishmania mexicana amastigotes: the role of cysteine peptidases and the NF-κB signaling pathway.* The Journal of Immunology, 2004. **173**(5): p. 3297-3304.

90. Martiny, A., et al., *Altered tyrosine phosphorylation of ERK1 MAP kinase and other macrophage molecules caused by< i> Leishmania</i> amastigotes.* Molecular and biochemical parasitology, 1999. **102**(1): p. 1-12.

91. Shaulian, E. and M. Karin, *AP-1 as a regulator of cell life and death.* Nature cell biology, 2002. **4**(5): p. E131-E136.

92. Schieven, G.L., *The biology of p38 kinase: a central role in inflammation.* Current topics in medicinal chemistry, 2005. **5**(10): p. 921-928.

93. Anderson, C.F., et al., *CD4+ CD25− Foxp3− Th1 cells are the source of IL-10–mediated immune suppression in chronic cutaneous leishmaniasis.* The Journal of experimental medicine, 2007. **204**(2): p. 285-297.
94. Van Assche, T., et al., *< i> Leishmania–</i> macrophage interactions: Insights into the redox biology.* Free Radical Biology and Medicine, 2011. **51**(2): p. 337-351.
95. Alvar, J., et al., *The relationship between leishmaniasis and AIDS: the second 10 years.* Clinical microbiology reviews, 2008. **21**(2): p. 334-359.
96. Giannini, M., *Suppression of pathogenesis in cutaneous leishmaniasis by UV irradiation.* Infection and immunity, 1986. **51**(3): p. 838-843.
97. Terabe, M., et al., *CD4+ cells are indispensable for ulcer development in murine cutaneous leishmaniasis.* Infection and immunity, 2000. **68**(8): p. 4574-4577.